



國立臺灣大學牙醫專業學院口腔生物科學研究所

碩士論文

Graduate Institute of Oral Biology

School of Dentistry

National Taiwan University

Master's Thesis

口腔癌酸化的臨床相關性及其對淋巴轉移的影響

Clinical Relevance of Oral Cancer Acidosis and its Implication on
Lymphatic Migration

林孟緹

Meng-Tie Lin

指導教授：周涵怡 博士

Advisor: Han-Yi Elizabeth Chou, Ph.D.

中華民國 113 年 2 月

February, 2024

誌謝



在碩班的這些日子讓我知道我有無限的可能，雖然曾經迷惘，也懷疑過自己的種種決定，但我認為是在台大口生所遇到的人事物，讓我對自己更有自信，也更了解自己想要的是什麼。而能有這樣的收穫，首先要感謝周涵怡老師對我的栽培，老師總是能跳脫框架、讓我一再的去反思，培養我清楚敘事和解決事情的能力！再來要謝謝品宣學姊在我每一個最需要的時刻伸出援手，陪我一起解決問題、看著我進步、陪我大哭又陪我大笑。還想特別感謝暄潔和乙綾兩位最得力的幫手，總是貼心的在左右關照著我，帶給我無限歡笑。謝謝在實驗室遇到的好夥伴們宛宜、阿圻、豐羽、貫今、彥青、Chelsea 和曜宇，好慶幸碩班生涯能待在氣氛這麼好的實驗室做實驗。

在研究的過程中遇到了很多的挑戰，如果沒有眾人的幫忙是不可能完成這篇論文的，想謝謝鄭世榮所長和珮瑤姊在搜集臨床檢體的各種支援；謝謝郭瑋庭老師於內皮屏障的實驗提供測量的儀器，還提供非常多寶貴的實驗建議；謝謝郭彥彬老師提供我們實驗室口腔癌細胞株；謝謝沈湯龍老師提供胞外體測量的儀器和試劑，且提供我們很多與胞外體學習相關的資源；謝謝在遠距教學課程指導我的李財坤老師，讓我們有機會能夠去跨國企業和各種展會參訪；謝謝共同實驗室 A 的學長姐總是能在需要時提供即時的幫助。也謝謝我的朋友們都無條件的相信我做得到，總是大聲告訴我我是最棒的！

最後想感謝最重要的爸媽以及一直鼓勵著我的哥哥和姊姊，家人們讓我沒有後顧之憂地完成學業，包容我在學校的時間比在家還多、還要兼顧玩樂（？ 但能這樣放肆是因為我知道家裡永遠為我留了一盞燈。

寫到這裡回頭看才發現已經變成一長串的名單，終於了解陳之藩先生所說的：「無論什麼事情，得之於人者太多，出之於己者太少，因為要感謝的人太多了，不如謝天吧！」噫！謝謝大家！我畢業啦！（大聲）

中文摘要



口腔癌在本國男性為第四常見之癌症，若轉移到淋巴，其五年存活率極低。根據實驗室先前研究成果得知，口腔癌微環境酸化與轉移密切相關。腫瘤微環境會透過不同因子影響腫瘤轉移，而胞外體作為生物體內訊息傳遞的工具，參與腫瘤和微環境之間的交互作用。然而，在口腔癌中，微環境對其胞外體分泌的影響尚未充分被了解。

本研究主軸是酸化微環境對口腔癌細胞的影響，除了實際搜集臨床口腔癌檢體以建立其即時測量酸鹼值方法外，我們也發現長期酸化之口腔癌細胞株具有大量釋放胞外體的特性，並進一步使用蛋白質體學和轉錄體學分析來研究其內容物。另一方面，我們將口腔癌胞外體添加至淋巴內皮細胞的培養基中進行刺激，使用跨膜電阻儀和免疫螢光細胞染色觀察內皮細胞之間的連結是否受到影響，並使用帶有螢光標記之葡聚糖測試內皮屏障之滲透度。根據實驗結果發現，酸化會造成口腔癌細胞釋放出大於正常酸鹼值的囊泡，且帶有不同蛋白質和 miRNA 內容物，這樣的細胞外囊泡具有破壞淋巴內皮細胞屏障的特性。結合臨床檢體的實際觀察和細胞實驗的證據，有助於更進一步了解酸化微環境所釋放的胞外體對口腔癌細胞轉移的潛力。

關鍵字：酸化微環境、口腔癌、胞外體、內皮屏障、緊密連結

ABSTRACT



Oral cancer ranks as the fourth most common cancer among men in Taiwan. Once it metastasizes to lymph nodes, the five-year survival rate becomes even lower than the tumor in situ. Based on previous research in our laboratory, we found that the acidotic microenvironment correlates to cancer metastasis by establishing the acidotic animal and cell line model.

Tumor metastasis is a complex process influenced by various factors, and one of these factors is the *in vivo* message transmission via extracellular vesicles, which participates in the reciprocal interaction between tumors and their metastatic site. However, the impact of acidosis on oral cancer metastasis remains largely unknown.

This study aims to evaluate the effect of oral cancer acidosis and its relationship with extracellular vesicle secretion and metastasis. We collected clinical oral cancer specimens and developed a protocol to obtain reliable pH measurements at the operation site. We isolated extracellular vesicles secreted by our long-term acidosis oral cell line model and found increased secretion and differential population as compared to its neutral pH counterpart. Subsequent proteomic and transcriptomic analyses were employed to analyze the contents of these extracellular vesicles. Also, we stimulated lymphatic endothelial cells with extracellular vesicles, then the integrity of the endothelial cell barrier was tested by transmembrane resistance using trans-epithelial electrical resistance (TEER) and immunofluorescence staining (IF). Furthermore, we used fluorescent-labeled dextran to interrogate the change in endothelial layer permeability after extracellular vesicle treatment.

In summary, our results show that acidosis oral cancer cells release more


extracellular vesicles, which contain distinct protein and miRNA contents. Moreover, these extracellular vesicles exhibit the capability to disrupt the lymphatic endothelial cell barrier. The amalgamation of our clinical observations, omics analyses, and functional experiments contribute to a more comprehensive understanding on the role of oral cancer acidosis in lymph metastasis in the context of extracellular vesicles.

Keywords: acidotic microenvironment, oral cancer, extracellular vesicles, endothelial barrier, tight junction.

CONTENTS

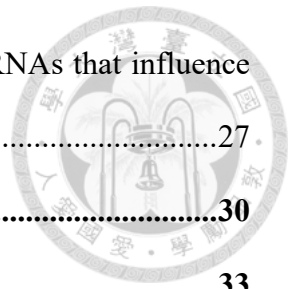


誌謝	i
中文摘要	ii
ABSTRACT	iii
CONTENTS	v
LIST OF FIGURES	viii
LIST OF TABLES	x
Chapter 1 Introduction	1
1.1 Oral Cancer	1
1.2 Microenvironment Acidosis.....	1
1.3 Extracellular Vesicles.....	2
1.4 Lymphatic Metastasis	3
1.5 Lymphatic Endothelial Cell-Cell Barrier.....	4
1.6 Hypothesis	4
1.7 Experimental Design	5
Chapter 2 Material and Methods	6
2.1 Clinical Data Collection and pH Value Detection	6
2.2 Cell Culture.....	6
2.2.1 Oral Squamous Cell Carcinoma.....	6
2.2.2 Lymphatic Endothelial Cell.....	7
2.3 Extracellular Vesicles Isolation.....	7
2.3.1 qEV Size Exclusion Chromatography (SEC).....	7
2.3.2 Tangential Flow Filtration (TFF)	8



2.4	Characteristics of Extracellular Vesicles	9
2.4.1	Nanoparticles Tracking Analysis (NTA)	9
2.4.2	Transmission Electron Microscope (TEM)	9
2.4.3	Proteomics Analysis	9
2.4.4	miRNA Extraction, RNA Library Construction and Sequencing	11
2.4.5	microRNA-seq Data Analysis	12
2.5	Endothelial Functional Assay	12
2.5.1	Trans Endothelial Electrical Resistance (TEER)	12
2.5.2	Immunofluorescence Staining	13
2.5.3	Permeability Assay	13
2.5.4	Extracellular Vesicles Labeling	14
2.6	Statistical Analysis	14
Chapter 3	Results	15
3.1	Correlation between the acidic microenvironment of oral cancer and tumor clinicopathology	15
3.2	The acidic microenvironment induces a more active interaction between oral cancer and the extracellular matrix	17
3.3	Characterization of extracellular vesicles released from oral cancer cell SAS under different pH microenvironments	18
3.4	Effects of acidification on proteomics of oral cancer cell extracellular vesicles	20
3.5	Characterization of SAS extracellular vesicles by tangential flow filtration under different pH conditions	23
3.6	Extracellular vesicles derived from SAS cells disrupt the endothelial integrity, especially under acidification	24

3.7	Extracellular vesicles at different pH values contain miRNAs that influence endothelial integrity	27
Chapter 4	Conclusion and Discussion	30
Chapter 5	Reference.....	33

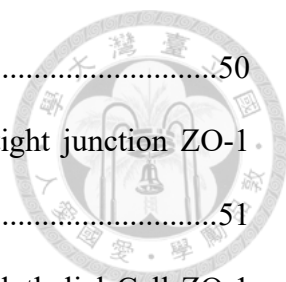


LIST OF FIGURES



Figure 1. Working setting for pH measurement of clinical oral cancer specimens	36
Figure 2. Clinical specimens show decreased pH value in the late stage of cancer	38
Figure 3. Extracellular vesicle biogenesis-related genes appeared in SAS cell transcriptome	39
Figure 4. Different characteristics of SAS-derived extracellular vesicles under different pH values.	40
Figure 5. The main population and minor population of pH6.6 EVs can be distinguished from nanoparticle tracking analysis.....	41
Figure 6. Acidification induces SAS to release the extracellular vesicles with different protein compositions.....	42
Figure 7. Extracellular vesicles secreted by SAS cells contain typical protein markers.	43
Figure 8. Top 10 enriched GO terms covering biological process, cellular component, and molecule function in SAS extracellular vesicles under different pH conditions.	45
Figure 9. Gene Ontology analyzes the protein function of pH 6.6 Minor.	46
Figure 10. Proteins that can promote EV internalization appeared in the pH6.6 minor group.	47
Figure 11. Characteristics of extracellular vesicle isolated by Tangential Flow Filtration	48
Figure 12. PKH Labeling shows Extracellular Vesicles Retention in Endothelial Cells Under Different pH Values.	49
Figure 13. Endothelial cells under EV treatment show no growth difference but different	

cytoskeleton organization.	50
Figure 14. Immunofluorescence staining revealed a disruption in tight junction ZO-1 expression in the extracellular vesicles-treated group.	51
Figure 15. Using Different Quantitation Methods of Lymphatic Endothelial Cell ZO-1 signals under Different pH values show the same trend.....	52
Figure 16. Evaluating the permeability of the lymphatic endothelial cell barrier through tracking FITC-dextran across the membrane.	53
Figure 17. Trans Endothelial Electric Resistance (TEER) detects the resistance of the endothelial barrier.	54
Figure 18. Differences in the composition of miRNA between 100kDa pH 7.4 and pH 6.6.	55
Figure 19. miRNAs specific target to ZO-1 appear in extracellular vesicles at both pH values	56



LIST OF TABLES



Table 1. Subject basic information37

Chapter 1 Introduction



1.1 Oral Cancer

Cancer stands as a significant global health problem. Based on the 111th annual causes of death statistics released by the Ministry of Health and Welfare in Taiwan, oral cancer ranks as the sixth most common cancer among the top ten and holds the 4th position among Taiwanese males. The incidence and mortality rates are remarkable. [1] Long-term chronic irritation is considered a primary cause of oral cancer, more specifically, Taiwan's unique dietary habits, including betel nut chewing, smoking, drinking, and extreme taste, all of these are recognized as potential contributors to oral cancer. [2-4]

Oral cancer is easily detected in the early stages with a five-year survival rate is over 70%-80%. However, if patients ignore symptoms or hesitating to the hospital and delay medical treatment due to worries, once the metastasis occurs, the survival rate will drop sharply to 30%. [5, 6] It's common to find oral cancer cell metastasis from mandibular lymph nodes to cervical lymph nodes in the late stage. It made the progress worse and worse. It's possible to metastasize to another organ such as the lung, bone, or liver.

1.2 Microenvironment Acidosis

A tumor microenvironment is a dynamic ecosystem surrounding a tumor. The interaction between tumor cells and their environment is important.

Hypoxia and acidosis are common characteristics in the tumor microenvironment. In detail, cancer cell induces changes in glucose metabolic mechanisms leading to an increase in the proportion of glucose glycolysis metabolism pathways to 85%, while only about 5% undergo aerobic respiration through mitochondria. This phenomenon, known

as the Warburg effect, was first proposed by Otto Warburg in 1925. [7, 8] The high metabolic demand of cancer cells results in the accumulation of H⁺ ions in the tumor microenvironment.

Various studies have confirmed that acidosis is correlated with angiogenesis[9], metastasis[10], immune resistance[11], and immunosuppression[12], all of the above may promote cancer progression [13]. It is noteworthy that Anemone et al. highlighted invasive breast cancer exhibits a more acidic tumor microenvironment, further leading to an increase in lung metastasis[14]. Lung tumor acidosis could not only increase cell proliferation and stemness but also promote metastasis progress, which was confirmed by our previous study. [15].

1.3 Extracellular Vesicles

Extracellular vesicles are nanoparticles released by both normal and pathological cells. They are categorized into apoptotic bodies, microvesicles, and exosomes based on their size. Exosomes range from 30 to 200 nm and were initially considered as biological waste bags. However, more and more research indicates that they serve as non-immunogenic carriers containing various biologically active molecules, including DNA, RNA, and proteins. [16] These vesicles play a crucial role in cell communication inside the body.

Studies have noticed that different tissue cells release extracellular vesicles that carry different kinds of content, serving as markers when cell metabolism is altered. [17]. Notably, exosome-mediated cell communication is not only within cells but also prolongs to tumor microenvironment. Tumor-derived exosomes enable the transfer of transforming growth factor beta (TGF- β) to normal fibroblast cells[18, 19]. 2016 study indicated that

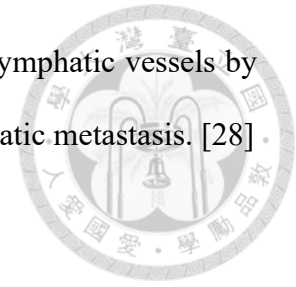
cancer-associated fibroblast-derived exosomes could modulate cancer cell metabolism mechanisms [20]. Besides their function in information transmission, extracellular vesicles can be isolated from any kind of body fluid, becoming a resource for biomarkers in tumor diagnosis and prognosis. This contributes to therapy and early detection and shows a significant potential application in this field. [21, 22].

1.4 Lymphatic Metastasis

Cancer metastasis is a major cause of poor progression, commonly attributed to either hematogenous or lymphatic metastasis. The mechanism of lymphatic metastasis typically involves penetrating the basement membrane of epithelial cells, traversing lymphatic vessels then spreading from the primary tumor site to a distant location. [2, 23]. Head and neck regions are abundant in lymphatic vessels, this brings anatomical advantages to oral cancer, and it is a key factor in oral cancer poor prognosis. Once metastasis happens, the patient's five-year survival rate decreases to 50%, and further metastasis becomes even lower than tumor in situ. [24]. This underscores the critical concern of metastasis.

Dr. Stephen Paget first introduced the "seed and soil" theory over a century, emphasizing that cancer metastasis cannot be due to chance. Cancer cells referred to as seeds, can only grow in proper soil, as known as a proper tumor microenvironment. [25, 26]. Recent studies have delved into the understanding of cancer cells preparing for future metastatic activities. These investigations reveal that metastasis activity does not occur by accident. In detail, cancer cell releases extracellular vesicles carrying certain molecules and attach to specific organs by the integrin on the vesicle surface to absorb these vesicles, so those extracellular vesicles could promote organ-specific metastasis. [27] Wang et al.

also noted in 2018 that cancer cells will promote the formation of lymphatic vessels by absorbing exosomes containing certain proteins, then causing lymphatic metastasis. [28].



1.5 Lymphatic Endothelial Cell-Cell Barrier

The lymphatic system plays a crucial role in the immune response and maintaining fluid balance. The structure of lymphatic vessels closely resembles that of blood vessels, both are connected and modulated by tight junctions and adherent junctions. Tight junctions are responsible for the regulation of paracellular permeability, while adherent junctions maintain vessel integrity through adhesive mechanisms. Notably, in epithelium, tight junctions and adherent junctions exhibit spatial distinction, while in endothelial cells, these junctions often intermingle. [29, 30] These proteins connect with the cytoskeleton and affect the integrity of the vessel wall

Breaking these junctions can lead to the attenuation of endothelial barrier function, alterations in wall permeability, and an increase in vascular permeability in disease. Numerous studies have highlighted that inflammation induces changes in cell connections, resulting in barrier dysfunction [31, 32]. The lymphatic system plays an important role in oral cancer metastasis, once it happens, cancer cells could break through the lymphatic vessel, migrating to neck region lymph nodes to establish colonization and growth. Among the processes, alteration of paracellular permeability is a significant factor, as cancer cells enter lymph vessels when the endothelial barrier is breached. [33, 34].

1.6 Hypothesis

1. Acidification may affect the characterization of extracellular vesicles released by oral cancer cell SAS.

2. Extracellular vesicles released by SAS may affect the lymphatic endothelial junctions and promote lymphatic metastasis.



1.7 Experimental Design

This study focuses on the impact of an acidic microenvironment on cancer cells. Combine clinical observation and in vitro cell acidosis model, inducing cancer cell release extracellular vesicles under different pH conditions. Next, clarify the characteristics and differences of these two types of extracellular vesicles. Furthermore, two types of extracellular vesicles are treated in lymphatic endothelial cells, and focus on their integrity, and permeability and observe the junction signal by immunofluorescence. Subsequently, proteins and RNA within the extracellular vesicles are analyzed using proteomics and next-generation sequencing. The aim is to comprehend the impact of exosomes secreted by oral cancer cells on the lymphatic metastasis of cancer cells in an acidic environment.

Chapter 2 Material and Methods



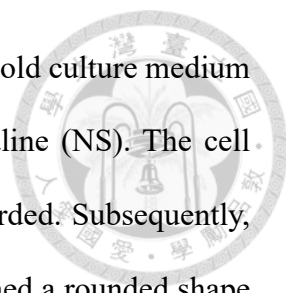
2.1 Clinical Data Collection and pH Value Detection

Clinical data and patient information collection were approved by the Institutional Review Board and National Taiwan University Ethics Committee and in cooperation with the Department of Dentistry of National Taiwan University Hospital. In three years, it is expected to collect 100 cases of oral cancer and 30 cases of impacted wisdom teeth, odontogenic cysts, or other intra-oral cases without oral precancerous lesions and no oral cancer diagnosis. The subjects are of any gender and their age ranges from 20 to 80 years old. Oral surgeon Dr. Shih-Jung Cheng performs all medical procedures and collects specimens. Immediately after the specimens are removed, a pocket-type pH meter (HORIBA pH meter) is used to measure the pH value, combined with the patient's information, and then processed Statistical analysis research. As of 2023, specimens from 29 oral cancer patients have been collected, and the mucosa and tumor surface were measured respectively. Taking into account the on-site conditions, if the specimen cannot be measured in time, the specimen will be brought back to the laboratory for measurement.

2.2 Cell Culture

2.2.1 Oral Squamous Cell Carcinoma

SAS, a low-aggressive human tongue cancer cell line was employed as the experimental cell line and cultured in DMEM (Dulbecco's Modified Eagle Medium) at pH 7.4/pH 6.6. The culture medium was supplemented with 10% FBS (Fetal Bovine Serum) and 1% PS (penicillin & streptomycin). Cells were cultured in 6 cm culture dishes



at 37°C in an atmosphere of 5% CO₂ in air. During subculturing, the old culture medium was initially aspirated, followed by washing with sterile normal saline (NS). The cell surface was rinsed with 0.025% trypsin-EDTA, aspirated, and discarded. Subsequently, the cells were returned to the incubator for 1 minute until they assumed a rounded shape and detached from the plate. Finally, the protease reaction was halted with the culture medium, and the cells were transferred to a culture dish containing fresh culture medium.

2.2.2 Lymphatic Endothelial Cell

Mouse Lymphatic endothelial cells, SVEC4-10 were procured from the Institute of Food Industry Development Bioresource Collection and Research Center (Taiwan, Hsinchu). The culture medium utilized was pH 7.4 DMEM with 10% EV-FREE FBS, and the culture process followed the aforementioned description.

2.3 Extracellular Vesicles Isolation

2.3.1 qEV Size Exclusion Chromatography (SEC)

Cells were cultured in 10 cm culture dishes, and 7 ml of DMEM medium (containing 10% FBS) was added to each culture dish. The cells were maintained in a 37°C, 5% CO₂ incubator, after one day, the cell medium was subsequently replaced with EV-Free DMEM medium (10% EV-FREE FBS). The cells were cultured for an additional two days, and the cell-conditioned medium was collected after reaching 80-90% confluence.

For the preparation of the supernatant, the cell medium was centrifuged at 200 x g for 3 minutes, followed by additional centrifugation at 300 x g for 3 minutes to remove floating cells. Subsequently, centrifugation at 2600 x g for 10 minutes was performed to eliminate cell debris and large apoptotic bodies. A final centrifugation at 16000 x g for 30

minutes was carried out to remove large microvesicles. The EV size range from 200 to 500 nm was then filtered out using a 0.22 μm filter to complete the preliminary centrifugation.

The cell culture medium was concentrated to less than 500 μl using a Millipore 100K concentrated centrifuge tube. Subsequently, a qEV SEC column (Izon Science) was employed to separate extracellular vesicles. Initially, 0.5 ml of the sample was added to the column, and 0.5 ml of the filtrate was collected as the first fraction. Then, 0.22 μm filtered normal saline (NS) was added, and the filtrate was collected in 0.5 ml increments up to the 15th tube. EV-SAVE (Fujifilm, Japan) was added to the 6th-13th tubes, and the extracellular vesicles were stored in a -80 degrees refrigerator.

2.3.2 Tangential Flow Filtration (TFF)

Select the appropriate filter membrane pore sizes, namely 100 kDa and 300 kDa (MidiKros® Filter Modules for volumes ranging from 100 ml to 3 L). The separation is achieved through a combination of size-exclusion-based physical sieving and chemical interaction with the membrane, facilitating the isolation of extracellular vesicles in the cell culture medium.

Install the Hollow Fiber and pump following the manufacturer's instructions, and introduce the cell culture solution that has undergone centrifugation at 2600 x g for 10 min and 16000 x g for 30 min into the sample bottle. Set the pump to test the initial flow of the Hollow Fiber at a flow rate of 100 ml/min. Subsequently, according to the guidelines, initiate the processes of concentration, liquid exchange, and re-concentration. Finally, clean the pipeline and Hollow Fiber with alkaline NaOH and store the samples in a -80 degrees refrigerator.

2.4 Characteristics of Extracellular Vesicles



2.4.1 Nanoparticles Tracking Analysis (NTA)

The extracellular vesicles isolated from cells were diluted with buffer. The Brownian motion of the vesicles was assessed using the NanoSight NS300® instrument (Malvern Panalytical, USA). The nanoparticles were subjected to excitation light, and the trajectory of the particles, represented by point scattering, was recorded to determine particle velocity. Subsequently, the velocity data were utilized to calculate both concentration and particle size.

2.4.2 Transmission Electron Microscope (TEM)

The 300-mesh Formvar- and the carbon-coated copper grid were discharged, and the exosomes were fixed with 2% paraformaldehyde for 1 minute. Subsequently, the grid was washed with ddH₂O. Following the washing step, the sample was stained with 2% Uranyl Acetate and dried for at least 30 minutes. The transmission electron microscope (Hitachi H-7650) was then utilized for observation.

2.4.3 Proteomics Analysis

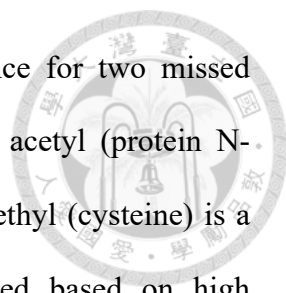
Proteomics analysis is conducted by the Chang Gung University Molecular Medicine Research Center, which employs gel-assisted digestion, LC-MS/MS analysis, and peptide-spectrum matching (PSM). The methodology is outlined as follows:

Gel-assisted digestion: Protein solutions are combined with SDS-PAGE sample buffer and heated at 95°C for 10 minutes. The proteins are then loaded onto and analyzed by 10% SDS-PAGE (1 cm) with Coomassie blue staining. The gel is destained and reduced with 10 mM dithiothreitol (DTT) at 60°C for 45 minutes, followed by cysteine-

blocking with 55 mM iodoacetamide (IAM) at 25°C for 30 minutes. Sequencing-grade modified porcine trypsin is used to digest the samples at 37°C for 16 hours. Peptides are extracted from the gel, dried by vacuum centrifugation, and reconstituted with 0.1% formic acid before analysis.

LC-MS/MS analysis: Digested peptides are diluted in HPLC buffer A (0.1% formic acid) and loaded onto a reverse-phase column (Zorbax 300SB-C18, 0.3 × 5 mm; Agilent Technologies). The peptides are desalted and separated on a homemade column (Waters BEH 1.7 μm, 100 μm I.D. × 10 cm with a 15 μm tip) using a multi-step gradient of HPLC buffer B (99.9% acetonitrile/0.1% formic acid) for 70 minutes with a flow rate of 0.3 μl/min. The LC apparatus is coupled with a 2D linear ion trap mass spectrometer (Orbitrap Elite ETD; Thermo Fisher) operated using Xcalibur 2.2 software (Thermo Fisher). Full-scan MS is performed in the Orbitrap over a range of 400 to 2,000 Da and a resolution of 120,000 at m/z 400. Internal calibration is performed using the ion signal protonated dodecamethylcyclhexasiloxane ion at m/z 536.165365 as a lock mass. Twenty data-dependent MS/MS scan events are followed by one MS scan for the 20 most abundant precursor ions in the preview MS scan. The m/z values selected for MS/MS are dynamically excluded for 40 seconds with a relative mass window of 15 ppm. The electrospray voltage is set to 2.0 kV, and the capillary temperature is set to 200°C. MS and MS/MS automatic gain control is set to 1,000 ms (full scan) and 200 ms (MS/MS), or 3 × 10⁶ ions (full scan) and 3,000 ions (MS/MS) for maximum accumulated time or ions, respectively.

Protein identification: Data analysis is conducted using Proteome Discoverer software (version 1.4, Thermo Fisher Scientific). The MS/MS spectra are searched against the SwissProt database using the Mascot search engine (Matrix Science, London, UK; version 2.5). For peptide identification, 10 ppm mass tolerance is permitted for intact



peptide masses and 0.5 Da for CID fragment ions, with allowance for two missed cleavages made from trypsin digestion. Oxidized methionine and acetyl (protein N-terminal) are considered variable modifications, while carbamidomethyl (cysteine) is a static modification. Peptide-spectrum matches (PSMs) are filtered based on high confidence and Mascot search engine rank 1 of peptide identification to ensure an overall false discovery rate below 0.01. Proteins with single peptide hits are retained.

2.4.4 miRNA Extraction, RNA Library Construction and Sequencing

Exosomal RNA extraction was performed at the Chang Gung University Genome Sequencing Platform. The procedure is outlined briefly as follows:

Before sequencing experiments, RNA concentration, purity, and integrity were evaluated using the RNA Nano 6000 Assay Kit on the Agilent Bioanalyzer 2100 System (Agilent Technologies, CA, USA). Illumina sequencing libraries were constructed using the NEXTflex™ small RNA-seq kit v3 Guide (Bioo Scientific, 5132-05), following the manufacturer's instructions. For each library, 60 ng of purified small EV RNA were ligated to 3' and 5' adaptors and then reverse transcribed to cDNA using adaptor-specific primers. After purification and PCR amplification using universal and specific barcode primers, the miRNA library was separated and retrieved from the 6% TBE-PAGE gel based on the corresponding size for miRNA distribution. The yield and size distribution of the small RNA libraries were evaluated using the Agilent 2100 Bioanalyzer instrument with the High-Sensitivity DNA Assay (Agilent Technologies). Each library, with equal concentration, underwent sequencing on a NextSeq 500 (Illumina) platform.

2.4.5 microRNA-seq Data Analysis

miRNA-seq data analysis is operated by Bioinformatics Core Laboratory, Molecular Medicine Research Center, Chang Gung University, the operation method is briefly described as follows: We processed microRNA-seq data using the Partek Flow analysis software (v10.0.21.1220). Initially, we removed low-quality bases and sequencing adapters from the raw FASTQ files. The trimmed reads were then aligned to the human reference genome (hg38) using Bowtie 2 (v2.2.5). Next, we quantified reads assigned to the miRNA listed in the miRBase (v22) and normalized them to CPM (Counts Per Million). Statistical analysis, hierarchical clustering, and differential expression analysis were performed using the GSA (Gene Specific Analysis) function in Partek Flow. We further analyzed the results using Qiagen IPA (Ingenuity Pathway Analysis, v101138820) to acquire target genes of each sequenced miRNA. The target genes derived from the differentially expressed miRNAs can be further explored for their potential role in biological processes or diseases.

2.5 Endothelial Functional Assay

2.5.1 Trans Endothelial Electrical Resistance (TEER)

Collagen-I (Corning, USA) was applied to the membrane of a 24-well Transwell plate, and lymphatic endothelial cells (SVEC4-10) were seeded on the insert. Upon reaching 90% confluence, the culture medium was replaced with 2% EV-FREE FBS DMEM. Using EVOM3 (WPI, USA), resistance values were measured and recorded at fixed daily time points over six days to assess cellular barrier resistance. The procedure is outlined as follows: Clean the electrode with alcohol, measure the resistance of the sample, and wait 1 minute and 30 seconds for the value to stabilize. After completing the

measurement, clean the electrode and record the value.



2.5.2 Immunofluorescence Staining

Using 4% paraformaldehyde, the Transwell membrane was fixed, and the cells were permeabilized using a permeabilization buffer for 5-10 minutes. Following permeabilization, the cells were immersed in a blocking buffer at room temperature for 30 minutes. Subsequently, the cells were incubated with primary antibodies: ZO-1 (1:750, Invitrogen, USA) for cell junction markers, Alexa Fluor 488 Phalloidin (1:500, Invitrogen, USA) for cytoskeleton staining, and DAPI (1:2000, Invitrogen, USA) for cell nuclei staining. After antibody incubation, the ZO-1 primary antibody was detected using the secondary antibody (1:500, Invitrogen, USA). Following a 1-hour incubation, the slide was mounted, and the status of cell connections was observed using an inverted microscope (Zeiss Observer D1, Germany).

2.5.3 Permeability Assay

A paracellular permeability tracer called 4-KD Fluorescein isothiocyanate-Dextran (Sigma-Aldrich, USA) is used. The flux from apical (AP) to basolateral (BL) can reflect the permeability of the cell monolayer. After removing the original culture medium from the Transwell, add HBSS/glucose containing 25 µg/ml 4-KD FITC-glucan and place it back in the incubator for incubation. After 9 hours, collect the BL side medium and use a microplate ELISA reader (BioTek Synergy HT, USA) to measure the fluorescence intensity of 100 µl of the medium under excitation light of 385 nm and emission light of 545 nm. Calculate the permeability between each specimen based on the fluorescence intensity of the BL side.

2.5.4 Extracellular Vesicles Labeling

5-10 μg of extracellular vesicles were mixed with Diluent C, bringing the sample volume up to 1 ml. Then, 6 μl of PKH26 dye was added to each sample, gently pipetted, and left at room temperature for 5 minutes. Next, quench the reaction by adding 2 ml of 10% BSA in PBS, bringing the total volume up to 8.5 ml.

Prepare the ultracentrifuge tube by adding 1.5 ml of sucrose solution to the bottom. Slowly layer the EV-PKH solution on top. Centrifuge at 190,000 G for 2 hours at 2-8°C. Upon completion of centrifugation, carefully aspirate the media and the interface layer, then resuspend the EV pellet in NS.

Transfer the EVs to a 10 kDa MWCO concentration tube, spin at 3000 x g for 10 minutes, and perform additional shorter spins as needed to reduce the volume to 0.5 ml. Utilize labeled EVs as soon as possible.

2.6 Statistical Analysis

All data were compiled in Excel (Microsoft Office, USA), and statistical analysis was conducted using GraphPad Prism 9 (GraphPad, Domatics, USA). Differences within and between groups were assessed using one-way ANOVA or Student's t-test. Gene Ontology was analyzed from an online database (<https://geneontology.org/>).

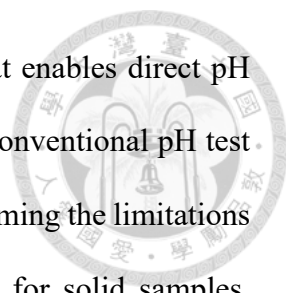
Chapter 3 Results



3.1 Correlation between the acidic microenvironment of oral cancer and tumor clinicopathology

Tumors develop a different metabolic pattern from ordinary cells. In addition to fueling tumor growth by producing necessary amino acids, cancer cells also produce excess acids. It has been reported that human solid tumors often have a high level of lactic acid accumulation [35]. In other research, Dario et al exhibited that highly invasive tumors have a relatively acidic pH value in the animal models of breast cancer. These results suggest a link between acidity and tumor metastasis [14]

We started a collaboration with oral surgeon Dr. Shih-Jung Cheng at the Department of Dentistry, National Taiwan University Hospital, to try to find out the relationship between tumors and the acidic microenvironment in oral cancer. We aimed to provide doctors with an indicator that can be used for diagnosis in the future and at the same time raise patients' awareness. We applied for IRB and tracked and collected affected area specimens from clinical oral cancer patients in the three years from 2022 to 2025. Comprehensive observation of laboratory cell experiments and comparison with clinical specimens. These specimens were clinically diagnosed oral cancer patients and comprised 100 cases of oral cancer and 30 specimens from patients with impacted wisdom teeth, odontogenic cysts, or other benign oral lesions without precancerous conditions, subjects' ages ranged from 20 to 80 years. In addition to acquiring tissue sections, saliva, blood, and medical records, we utilized a pocket-type pH probe (HORIBA pH meter) for real-time pH measurement during tissue extraction. (Figure 1A) If it is a traditional pH value measurement, the sample must be in the liquid, which is difficult to do in the operating



room. This pH meter offers a membrane-shaped measuring area that enables direct pH measurement of dry samples as small as 0.5x0.5 cm², compared to conventional pH test papers, this probe offers a more objective measurement which overcoming the limitations of traditional pH instruments that are cumbersome and unsuitable for solid samples. Moreover, it is lightweight, user-friendly, and portable to surgical sites for immediate measurements after calibration (Figure 1B) To date, we have collected data from 29 cases, including basic information like age, gender, smoking and betel nut chewing habits, and cancer stage. We compared tumor and adjacent normal tissue pH values based on the oral surgeon-diagnosed tumor size (T) stage (Table 1) after excluding 5 cases with diagnoses other than oral cancer. At the same time, the pH value of the oral mucosa was also measured to understand the relationship between oral cancer size and acidification, aimed to obtain clues to help oral surgeons evaluate.

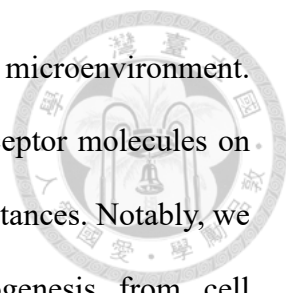
The comparison parts of the specimens are illustrated in Figure 2A, divided into the tumor side, adjacent normal side, and mucosa of the two groups. We further excluded eight treated cases and analyzed the correlation between tumor size and tissue pH value. The results show that on-site measurements in the operating room (OR) revealed a downward trend in pH values in larger-size tumors and were not observed when the tumors were smaller. In addition, it can be observed that the distribution of values measured in the laboratory is relatively chaotic and has no specific trend. This is because the tumor microenvironment is an open space and will be affected by tissue fluid and post-excision air. (Figure 2B) At the same time, we also measured the mucosal pH and revealed the relationship between pH value and tumor size, which had the potential to be developed into a practical outpatient measurement model in the future. The pH values were slightly lower than those of normal mucosal tissue in the larger size, while this phenomenon is less apparent in the smaller tumor. Even with a limited number of samples,

these trends persisted, emphasizing the importance of on-site pH measurements during specimen extraction. (Figure 2C). To sum up, based on our previous investigations and clinical case observations, both in vitro and in vivo experiments consistently highlight acidification as a physiologically relevant process that stimulates cellular changes and the release of specific signals. This phenomenon is evident in clinical specimens, revealing pertinent trends.

3.2 The acidic microenvironment induces a more active interaction between oral cancer and the extracellular matrix

In our lab, we concentrated on the impact of the acidic microenvironment on cancer progression. To understand the effects, we established long-term acidified oral cancer cell models and animal models which demonstrate that acidification stimulation enhances cell stemness and increases resistance to drugs. These findings have been validated in lung cancer and oral cancer, as reported in the paper published. [15]

Based on this research, we used GeneOntology to analyze the SAS cell transcriptome, to understand what are the most significant genes that participate in SAS cells under acidification. (Figure 3A) It reveals 360 genes with significantly differential expression from over 10,000 transcriptomes under acidification, using criteria of fold change>|2|, p-value<0.05 to categorize their Biological Process, Cellular Component, and Molecular Function. We found some significantly different Biological Process, including cell communication, regulation of cell secretion, and message transmission, were up-regulated. In the Cellular Component, interactions with the extracellular matrix, cells, and the external environment were significantly increased, indicating SAS cells were



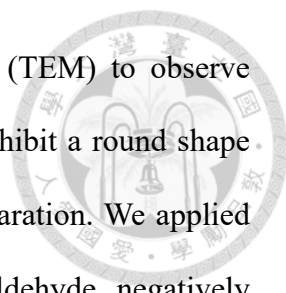
uninterrupted communication between tumor cells and the outside microenvironment. Finally, in Molecular Function, we found an increase in various receptor molecules on the cell membrane which directly interacted with other cells and substances. Notably, we identified some genes related to the extracellular vesicle biogenesis from cell communication, regulation of secretion, and signaling, such as WNT7A, RAB3A, WHT5B, TRPM4, and RhoBTB1. From the volcano plot, these genes were all up-regulated (Figure 3B) These results suggest that acidified oral cancer cells SAS exhibit increased activity in communicating with the external environment. Extracellular vesicles are one of the prominent ways.

3.3 Characterization of extracellular vesicles released from oral cancer cell SAS under different pH microenvironments

In 2015, Shen et al. pointed out that extracellular vesicles released by tumor cells will determine the direction of future metastasis of cancer cells, which is called tropism [27]. In addition, in oral cancer, it was also found that the secreted extracellular vesicles would bind to cells through specific receptors Laminin332 on the membrane and promote the formation of lymphatic vessels and the process of metastasis. [28] Few addresses how the acidic microenvironment impacts extracellular vesicles released by oral cancer cells and how these vesicles affect cancer progress. The results remain unclear. For this study, we used the tongue cancer cell line SAS as a model to isolate cancer cell extracellular vesicles. The cells were cultured at a concentration of 1×10^6 /ml under two different pH conditions - normal physiological pH (pH 7.4) and an acidic environment (pH 6.6). We observed their morphological characteristics and growth status. Figure 4A illustrates the

cells grew normally in both pH conditions, forming colonies that extended into sheets. Afterward, we isolated extracellular vesicles released by the cells under different pH values.

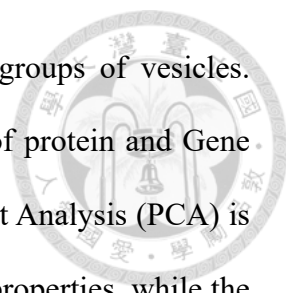
There are different ways to isolate extracellular vesicles, one method is ultrahigh-speed centrifugation which separates vesicles based on their density. Another method is immunoaffinity capture which targets specific surface proteins. In this study, we use Size-exclusion chromatography (SEC), a gravity-based method that separates vesicles by their size. It works by allowing particles of different sizes to pass through pores and facilitates the separation of vesicles. We found that SEC was effective in generating high-purity, intact extracellular vesicles. SAS cells were cultured in cell culture plates at a concentration of 1×10^6 /ml under normal physiological pH (pH 7.4) and acidification (pH 6.6) medium. We collected a quantitative amount of cell culture medium followed by high-speed centrifugation to discard the cell debris, then went through Size-Exclusion Chromatography to separate extracellular vesicles. Subsequently, nanoparticle tracking analysis (NS300) was employed to measure particle size and concentration (Figure 4A). Extracellular vesicles secreted under normal physiological pH 7.4 exhibited an average size of approximately 113 nm and its concentration corresponds to the y-axis is about 5×10^8 , which is equivalent to each cell producing 2.5×10^8 113nm EVs. Similarly, under acidic conditions (pH 6.6), extracellular vesicles from acidified SAS cells had an average size of about 125 nm. In our study, we found that SAS cells tend to secrete more extracellular vesicles after being stimulated by acidification. and multiple subpopulations appear compared with normal physiological pH values. Extracellular vesicles exhibited additional subpopulations with sizes of 63 nm and 205 nm at pH 6.6 condition (Figure 4A). We found that oral cancer cells tend to release more, and slightly larger vesicles under acidification.



At the same time, we use transmission electron microscopy (TEM) to observe extracellular vesicle morphology. Extracellular vesicles typically exhibit a round shape or a cup-shaped appearance due to dehydration during sample preparation. We applied EV onto a carbon-coated copper grid, fixed it with 2% paraformaldehyde, negatively stained it with 2% uranyl acetate, and analyzed it using a transmission electron microscope. As shown in Figure 4B, at pH 6.6, the size of the vesicles isolated by SEC is slightly less than 100nm, and vesicles of different sizes can be observed in the same field of view, which is consistent with the measurement by NTA, while other larger field of view, classic cup shape caused by dehydration can also be observed.

3.4 Effects of acidification on proteomics of oral cancer cell extracellular vesicles

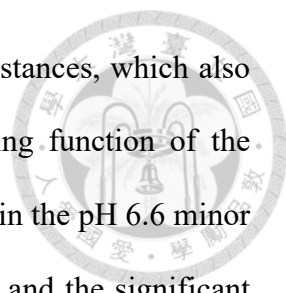
It has been confirmed that external factors such as hypoxia or inflammation can alter the characteristics of extracellular vesicles released by cells. We observed a similar phenomenon in our study with SAS oral cancer cells. These cells release groups of extracellular vesicles, and after being subjected to acidic stimulation, a subpopulation with a size of approximately 60 nm emerged. This piqued our curiosity about the post-acidification subpopulation. (Figure 6A). We can use the NTA fractions to separate the pH6.6 subpopulations generated by acidification. We can pool the 7th and 8th tubes to get the group of vesicles with a size of about 125nm, called "pH 6.6 Major", and then pool the 9th and 10th fractions together to separate another group with a size of about 63 nm is called "pH 6.6 minor" (Figure 5B). Three groups of vesicles, pH 7.4, pH 6.6 Major, and pH 6.6 minor, will be analyzed by the Molecular Medicine Research Center of Chang Gung University to analyze the protein contents and abundances in the extracellular vesicles under the same number of vesicles.



Then use LC-MS/MS to identify the content of these three groups of vesicles. Followed by a Venn diagram and PCA to analyze the distribution of protein and Gene Ontology was used to analyze protein function. Principal Component Analysis (PCA) is shown in Figure 6A, pH6.6 Major and pH 7.4 have relatively close properties, while the pH 6.6 minor group has different protein composition, which implies that oral cancer secret vesicles of different sizes carry different messages. 581 proteins were detected in SAS pH7.4 and pH6.6Major and pH6.6minor EV, 386 proteins were detected in pH7.4, 418 proteins were detected in pH6.6Major, and 529 proteins were detected in pH 6.6 minor. (Figure 6B) There is a significant overlap between the three samples. Comparing the pH7.4 and pH6.6 groups, 155 (122+46+27) specific proteins only appeared in the pH6.6 population, as many as 122 proteins appear in the pH 6.6 minor group, which is different from the protein inclusions in the pH7.4 and pH6.6 Major groups.

The most commonly recognized extracellular transmembrane proteins CD81, CD63, and CD9, as well as common heat shock proteins HSP70, HSP90, etc., were found among the 324 proteins common to the three, which can indicate the accuracy of the vesicle isolation results. Among them, we found that pH 6.6 minor has the highest protein abundance. (Figure 7)

We use Gene ontology analysis to investigate the vesicles under two different pH environments. This analysis focuses on biological processes, cellular components, and molecular functions, providing a more comprehensive understanding of the composition of SAS cell-derived extracellular vesicles. It was observed in the cellular component category that the components of Extracellular exosomes accounted for the largest amount in any group (Figure 8). The three groups of proteins have been analyzed a great overlap and similar functions. Special terms are still found among them, for example, the function of virus receptor activity appears in the pH6.6 minor group. This category includes many



receptor-related proteins that are related to the entry and exit of substances, which also implies that the protein components in EVs will affect the docking function of the recipient cells. We further explore what kind of proteins only appear in the pH 6.6 minor group. 122 proteins were selected and analyzed by Gene Ontology, and the significant biological processes, molecular functions, and cellular components were selected through $p < 0.05$. It was found that among the proteins of pH 6.6 minor, many proteins interact with the extracellular matrix, and there are also some proteins responsible for cell adhesion and organizing collagen. In addition to the majority of proteins related to extracellular vesicles, cellular components related to the extracellular space can also be observed in the function of cell composition. The molecular function of the pH6.6 minor protein is to contribute to the structural integrity of the extracellular matrix, and they have enzyme catalytic activity and functions related to binding to cell adhesion molecules. (Figure 9)

Previous studies have pointed out that the head and neck contain abundant lymphoid tissue, which has the physiological location advantage of oral cancer invasion and metastasis. oral cancer releases extracellular vesicles containing Laminin r3, which binds to endothelial cell membranes through integrin $\alpha 3$, promoting the uptake of extracellular vesicles[28]. We also discovered that pH 6.6 Minor revealed the Laminin r3 signal and it is higher than pH 7.4, which probably attracted more pH 6.6 minor extracellular vesicles and endothelial cells in subsequent cell experiments (Figure 10).

Based on the above, it can be found that pH6.6 minor protein contents and functional tendencies affect the interaction with the extracellular matrix through the function of catalytic enzymes, and may also regulate adhesion-related functions, making it easier for other proteins or subjects to conduct and achieve physical changes in cell structure or extracellular matrix. This coincides with the observation in previously analyzed SAS cell transcriptome results that cells tend to interact with the extracellular matrix.

3.5 Characterization of SAS extracellular vesicles by tangential flow filtration under different pH conditions

Highly pure and intact vesicles can be isolated by size-exclusion chromatography (SEC), but one limitation is its inability to produce the same quality and quantity of extracellular vesicles required for subsequent experiments. To address this constraint, we subsequently employed the Tangential Flow Filtration (TFF) separation method. TFF is a fully sealed automated system that utilizes a circulation method to filter out contaminant content through pores of varying sizes, making it the largest volume cell culture fluid processing method. According to the varied acidification extracellular vesicle population distributions observed from SEC results, here, we opted for two kinds of columns with different pore sizes, which are 100kDa and 300kDa. Both membranes can separate particles within the size range of 100 kDa: 30-220 nm and 300 kDa: 100-220 nm. The EVs isolated by the 100 kDa column can include the pH 6.6 subpopulation, so our subsequent cell experiments will utilize 100 kDa EVs. From the results shown in Figure 11A, it was observed that among the 100 kDa vesicles isolated, the most significant vesicle size was around 73 nm under both pH values. Many small groups were isolated, such as a group of vesicles ranging from 104-128 nm and a group with a size around 58 nm. The particle distributions of the two methods are different; TFF separates EVs based on hole size, while size exclusion uses the swimming paths of the particles to separate EVs of different sizes. Here, we specifically chose the method that can separate small EVs. Thus, the presentation of TFF may result in the same distribution for both pH values.

NTA is performed to measure the size and concentration of EVs, and TEM was also used to observe the appearance of EVs (Figure 11B). Most of the pH 7.4 vesicles isolated using TFF are smaller than those observed by SEC, with a size of about 50-60 nm,

exhibiting small round shapes, and cup-shaped structures can also be observed. The edges of pH 6.6 vesicles are less rounded, but this may also be caused by the specimen preparation. Whether extracellular vesicles are isolated by SEC or TFF, typical round or cup shapes can be observed under a transmission electron microscope, and their sizes are consistent with the size range measured by NTA.

3.6 Extracellular vesicles derived from SAS cells disrupt the endothelial integrity, especially under acidification

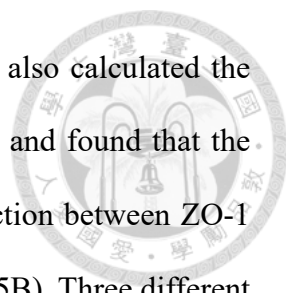
We want to understand whether EVs secreted by acidified oral cancer cells will affect lymphatic endothelial cells. We already know that cancer cells most often infiltrate through lymph when they want to metastasize, and the connection between endothelium determines the ease of cell infiltration. Epithelial cells and endothelial cells are linked in a sheet-like manner. Tight junctions, adherens junctions, and desmosomes are involved in the linkage. In addition to their connecting functions, tight junction proteins function as regulators of paracellular ion permeability and maintain cell polarity. Numerous studies have implicated that cancer extracellular vesicles are not only involved in the tumor metastasis process but also break through the barrier to establish the pre-metastatic niche. However, existing research has predominantly focused on blood vessels or the gastrointestinal tract and the blood-brain barrier. There are relatively few investigations into the lymphatic barrier which exhibits the highest oral cancer metastatic rate.

We used mouse lymphatic endothelial cells SVEC4-10 and treated PKH labeling EVs on endothelial cells. It was found that after PKH-EV treatment after 24 hours, the retention phenomenon of EVs is different at pH 7.4 and pH 6.6. Lymphatic endothelial cells tended to retain EVs in the cells after internalized EVs at pH 6.6, and this phenomenon was not observed at pH 7.4. (Figure 12A) This situation can be illustrated

by the percentage of PKH-positive cells and the intensity of overall EV-PKH (Figure 12B).

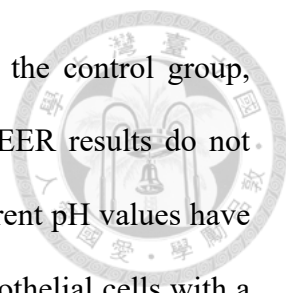
Next, to determine whether oral cancer in an acidic microenvironment releases extracellular vesicles that can destroy the lymphatic endothelial barrier function, fluorescent staining was used to observe the morphology of the cells, and Phalloidin was used to observe the cytoskeleton. It was found that there was no problem with the cell growth and the number was also about the same. However, under the conditions of a lower magnification field of view, it was found that when the number of cells was similar, the cell cytoskeleton expansion of pH 6.6 seemed to be affected, and it appeared elongated. (Figure 13A) From the high-magnification field of view and when the cell density reached confluence, the control group without EV addition showed obvious cell boundaries and skeleton signals, compared to the EV-treated group, the signal at the cell junction was somewhat unclear (Figure 13B), so we speculated that the connection between cells may be affected.

To verify this situation, we further used Anti-ZO-1 as a marker of tight junctions to observe the tight junctions, here we also used Phalloidin to observe cytoskeletal actin and used DAPI to observe the position of the nucleus. From the staining results, it was found that the control group showed a complete ZO-1 signal and the same results could be seen under different visual fields. However, there was a difference between the endothelial cells treated with pH 7.4 and pH 6.6 EVs. Many incomplete boundaries were observed, and the pH6.6 group had more severe ruptures (Figure 14A). Through quantification of fluorescence signals in multiple fields of view, the pH6.6 group produced a lower fluorescence intensity than the other two groups (Figure 14B). Further calculation of cells with complete borders in several fields of view also yielded similar results. The control group had the most complete cell borders, while the pH7.4 and pH6.6 groups had more cells with incomplete borders. (Figure 15A) Since the tight junction protein is not a



continuous signal, it is presented in a point-to-point manner, so we also calculated the number of breakpoints generated between edges at the same length and found that the pH6.6 group has the highest number of breakpoints, and the connection between ZO-1 appears fragmented compared to pH7.4 and control groups (Figure 15B). Three different quantitative methods and the presentation of fluorescence images have pointed out that extracellular vesicles contain factors that affect endothelial connections. Among them, the extracellular vesicles secreted by oral cancer cells under acidification have a greater impact on the barrier between lymphatic endothelial cells, which may result in increased permeability. Such evidence tells us that the possibility of cancer cell metastasis is greatly increased when the barrier is loose. From the results of fluorescent staining, we found that there is a connection problem with the tight Junction of lymphatic endothelial cells, which will also affect the permeability of the cells, so we used Dextran-FITC 4kDa with a size of about 2.8 nm, which is a paracellular permeability tracker. By allowing the fluorescent particles to penetrate the endothelial barrier, the flux from Apical to basolateral can reflect the permeability of the monolayer cells. After nine hours of treatment, it was found that the group treated with extracellular vesicles had significantly more fluorescent signals in the lower chamber than the control group and pH7.4 group. Among them, pH 7.4 and pH 6.6 were more effective. It can be seen that the fluorescence signal of the pH6.6 group is significantly higher in the wells in the basolateral (Figure 16). This result implies that the pH6.6 treated group may have more or larger gaps.

Finally, we utilize transendothelial electrical resistance (TEER, EVOM3) to apply a 12.5 AC through a monolayer without causing cell damage. We measure the resistance value generated by tightly sealed endothelial cells, which reflects the tightness of the endothelial barrier. Subsequently, we expose the endothelial cells to extracellular vesicles to observe their effects on lymphatic endothelial cells. According to the TEER results,



endothelial cells treated with EVs exhibit looser connections than the control group, resulting in lower resistance values (Figure 17A). However, the TEER results do not elucidate the differential effects that extracellular vesicles with different pH values have on endothelial cells. To address this, we considered that treating endothelial cells with a large amount of EVs at once does not replicate the physiological conditions of EV release by cells. Therefore, we designed a regimen to reduce the dose and administer EV treatment in three doses. Surprisingly, after the second EV boosting on Day 3, the resistance value was measured the next day. There was a significant difference between pH 6.6 and pH 7.4, with pH 6.6 demonstrating the ability to disrupt cell barriers, resulting in lower resistance values compared to the pH 7.4 treatment and the control group (Figure 17B). This indicates that extracellular vesicles isolated from cancer cells may contain certain contents that affect tight junctions and cause disruption, consistent with previous literature.

3.7 Extracellular vesicles at different pH values contain miRNAs that influence endothelial integrity

Our cell experiments not only revealed that acidified oral cancer cells release extracellular vesicles with different profiles but also confirmed that the barrier is damaged by these vesicles. These results have raised our curiosity about the factors involved. In the proteomic analysis, we observed that most of the functions are related to cell adhesion or interaction with the extracellular matrix, with few clues about tight junction destruction. We speculate that this may be influenced at the miRNA level.

To investigate further, we engaged the Next Generation Sequencing Center of Chang Gung University to perform miRNA sequencing on extracellular vesicles, aiming to

identify miRNAs that disrupt barriers or induce cytoskeleton remodeling. The analysis revealed 408 miRNAs and the Heatmap and PCA analysis results displayed in Figure 18 illustrate differences between miRNAs at pH 7.4 and pH 6.6.

During our cell experiments, we observed that EVs contribute to the disruption of the endothelial tight junction protein ZO-1. Consequently, we initially focused on miRNAs specifically targeting ZO-1. However, both groups showed miRNAs regulating ZO-1, but there was no apparent difference in abundance (Figure 19A).

Subsequently, we identified 77 differentially expressed miRNAs from the 100kDA group under $p > 0.05$ and $\text{Fold change} > |2|$ criteria. Then, investigate the genes targeted by these miRNAs and find out the pathways they participate in from the Ingenuity Pathway Analysis (IPA) database. Eight miRNAs with significant differences between pH6.6 and pH7.4 were identified (Figure 19B): miR1-143p, miR-134-5p, hsa-miR-29c-3p, hsa-miR-106b-5p, hsa-miR-34c-5p, hsa-miR-30e-5p, hsa-miR-363-3p, and hsa-miR-1-3p. The four proteins with higher expression at pH 6.6—miR141-3p, miR-134-5p, hsa-miR-29c-3p, and hsa-miR-106-5p. Among these, miR141-3p is a member of the miR200 family, which is associated with cell adhesion, motility, and binding, especially function in regulating tight junctions[36, 37]. miR106b-5p targets the PTEN pathway in breast cancer, known for inhibiting PI3K-Akt-dependent cell proliferation and migration[38, 39]. miRNA29c-3p is linked to endothelial cell apoptosis and has been shown to promote angiogenesis and increase vascular permeability.[40] miRNA134-5p overexpression is associated with lung adenocarcinoma metastasis and resistance to chemotherapy drugs. [41, 42] The four proteins with high expression in pH7.4—hsa-miR-34c-5p, hsa-miR-30e-5p, hsa-miR-363-3p, and hsa-miR-1-3p—affect endothelial connections. Studies show that miR34c overexpression damages the blood-tumor barrier[43], miR30e-5p regulates PFN2, which regulates the cytoskeleton organization in head and neck

cancer[44], miR363-3p acts as a tumor suppressor in clear renal cell carcinoma[37, 45], and miR1-3p influences the EMT process in renal cell carcinoma and increases the permeability of HUVEC[46].

In addition to the miRNAs that affect tight junction expression, EVs released by oral cancer also contain miRNAs that influence endothelial junctions and contribute to tumor metastasis. Apart from directly regulating ZO-1, these miRNAs may indirectly affect ZO-1 by targeting other genes, leading to significant junction damage at pH 6.6. This aspect represents a crucial area for future in-depth investigation.

Chapter 4 Conclusion and Discussion



The acidic environment plays a crucial role in tumor development and directly impacts various biological processes in the tumor microenvironment. Our previous research revealed that external stimulation can cause physiological changes even in the same cells. In detail, cancer cells exhibit stemness and drug resistance, as well as altered transcriptomes and proteome composition after acidic stimulation [15]. Building upon this study, we aim to further explore the disparities between extracellular vesicles released by oral cancer cells following acidification stimulation and those released in a normal environment. We are also curious about the function behind the vesicles, so we investigate the impact of these vesicles on lymphatic endothelial cells, with a particular focus on barrier dysfunction.

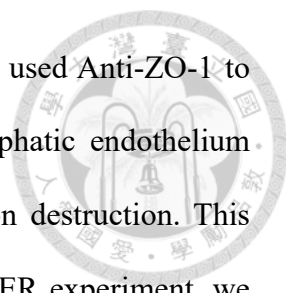
Connecting the laboratory to the clinical part, we earned to explode for methods enabling rapid pH detection to aid clinicians in diagnosing cancer in the early stage. In this context, we attempted to employ a pocket pH meter for measurements, revealing lower pH values in tumor specimens from clinical subjects, particularly in patients with larger tumors. This phenomenon showed that this method is feasible and notably appeared in real-time surgical specimen removal. Such findings reinforce our belief in the non-negligible impact of acidification on tumors. We established an acidified oral cancer cell model, SAS. Stimulate the cells under the tumor microenvironment of pH 6.6 and an environment of pH 7.4 to simulate the peripheral neutral pH value area of the tumor.

Our results indicated that acidification stimulation indeed alters the extracellular vesicles released by cells. Not only the vesicle's characteristics but also its contents. Acidification induces cells to secrete more and slightly larger extracellular vesicles. Particularly, our study observed that acidification also modifies the population

composition of extracellular vesicles, especially those of smaller size groups. Such small groups can be separated by pooling different fractions of size exclusion. However, due to the initial inexperience in using TEM, only the pH 6.6 group was shown in Figure 4, and the pH 7.4 group was not photographed.

We identify the composition of vesicle contents was different from those of vesicles in a normal pH environment through proteomics and transcriptomics analyses. It was observed that EVs of similar sizes have relatively similar protein contents from the PCA results, and most proteins in the three groups share similar compositions, which engage in functions related to extracellular matrix regulation and adhesion. Among these three, the pH 6.6 Minor group exhibited distinctive features associated with membrane regulation of transmembrane channels for foreign substance entry and exit.

We focus on the pH 6.6 minor group, and our research has revealed unique protein functionalities that affect interactions with the extracellular matrix. These functionalities are related to catalytic enzyme functions, which may regulate adhesion-related functions and facilitate the movement of substances into and out of cells. To ensure that there is a sufficient amount of EVs for subsequent experiments, we used TFF to isolate extracellular vesicles of obtain consistent quality from the same batch and used a 100kDa column with a smaller pore size to include the pH 6.6 Major and pH 6.6 minor groups previously observed. After the characteristics of extracellular vesicles, we treated the vesicles in lymphatic endothelial cells SVEC4-10. First, PKH26 was used to label EVs in endothelial cells, and it was found that the pH 6.6 group has more retention ability in cells. Then, we aimed to realize what would happen after EV treatment, we used phalloidin to label the cytoskeletal actin, the immunofluorescence image showed that cell growth was not affected, but the growth of the cytoskeleton seemed to be restricted, and blurry signals appeared at the boundaries of the cells. Therefore, we suspected that the cell barrier was



affected. To observe the changes in the endothelial cell barrier, we used Anti-ZO-1 to highlight the tight junctions. Surprisingly, we found that the lymphatic endothelium treated by extracellular vesicles had significant ZO-1 tight junction destruction. This phenomenon is more significant in the pH 6.6 group. From the TEER experiment, we demonstrated high-dose EV treatment and found that the EV-treated group had a lower resistance value than the control group, but the TEER results did not clearly explain the differential effects that two extracellular vesicles. Therefore, we used a low-dose and multiple-boosting model to simulate physiological conditions and found the barrier destruction effect of the EV-treated group, especially pH 6.6, was more significant.

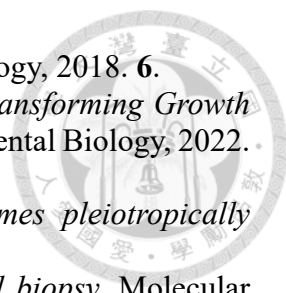
Additionally, Proteomics results demonstrated that extracellular vesicles are enriched with proteins associated with adhesion, cytoskeleton reorganization, and enzyme catalysis. At the level of miRNA, we also found a miRNA that specifically targets the ZO-1 protein, but there is no significant difference between the two groups, so we suspected that besides the way that miRNA directly regulates ZO-1, it may also indirectly affect ZO-1 by regulating other genes, thereby causing such a huge junction disruption at pH 6.6.

Future experiments can consider identifying other genes that indirectly affect ZO-1, treating target proteins that affect endothelial integrity through knockout (KO) experiments, and further testing whether the ZO-1 junction protein signal is recovered. In terms of animal models, it can be explored whether mice with tumor cells accelerate metastasis due to extracellular vesicles and whether the number or size of metastatic lesions are affected. In terms of clinical application, we have to continue collecting clinical tumor pH values and conduct larger-scale statistical analysis to provide more accurate clinical diagnosis and treatment guidance.

Chapter 5 Reference

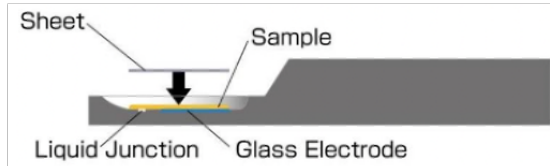


1. Welfare, M.o.H.a., *111 年國人死因統計結果-分析*. 2023.
2. Bugshan, A. and I. Farooq, *Oral squamous cell carcinoma: metastasis, potentially associated malignant disorders, etiology and recent advancements in diagnosis*. F1000Research, 2020. **9**: p. 229.
3. Gupta, A.A., et al., *Chronic mechanical irritation and oral squamous cell carcinoma: A systematic review and meta-analysis*. Bosnian Journal of Basic Medical Sciences, 2021.
4. Johnson, D.E., et al., *Head and neck squamous cell carcinoma*. Nat Rev Dis Primers, 2020. **6**(1): p. 92.
5. Chou, H.C., et al., *Clinical outcomes of oral cancer patients who survive for more than 5 years in Taiwan*. J Formos Med Assoc, 2019. **118**(12): p. 1616-1622.
6. foundation, F.c. *Oral Cavity Cancer*. 2022; Available from: <https://www.canceraway.org.tw/cancerinfo.php?id=D0052AC3-BE9A-46BC-B9F4-164FF14F3BF9>.
7. Warburg, O., *The Metabolism of Carcinoma Cells*. The Journal of Cancer Research, 1925. **9**(1): p. 148-163.
8. Wang, Y. and G.J. Patti, *The Warburg effect: a signature of mitochondrial overload*. Trends in Cell Biology, 2023. **33**(12): p. 1014-1020.
9. Wicks, E.E. and G.L. Semenza, *Hypoxia-inducible factors: cancer progression and clinical translation*. Journal of Clinical Investigation, 2022. **132**(11).
10. Pillai, S.R., et al., *Causes, consequences, and therapy of tumors acidosis*. Cancer and Metastasis Reviews, 2019. **38**(1-2): p. 205-222.
11. Barnes, E.M.E., et al., *Lactic acidosis induces resistance to the pan-Akt inhibitor uprosertib in colon cancer cells*. British Journal of Cancer, 2020. **122**(9): p. 1298-1308.
12. Dutta, S., et al., *Targets of Immune Escape Mechanisms in Cancer: Basis for Development and Evolution of Cancer Immune Checkpoint Inhibitors*. Biology, 2023. **12**(2): p. 218.
13. Pérez-Tomás, R. and I. Pérez-Guillén, *Lactate in the Tumor Microenvironment: An Essential Molecule in Cancer Progression and Treatment*. Cancers, 2020. **12**(11): p. 3244.
14. Anemone, A., et al., *Tumour acidosis evaluated in vivo by MRI-CEST pH imaging reveals breast cancer metastatic potential*. British Journal of Cancer, 2021. **124**(1): p. 207-216.
15. Shie, W.-Y., et al., *Acidosis promotes the metastatic colonization of lung cancer via remodeling of the extracellular matrix and vasculogenic mimicry*. International Journal of Oncology, 2023. **63**(6).
16. Herrmann, I.K., M.J.A. Wood, and G. Fuhrmann, *Extracellular vesicles as a next-generation drug delivery platform*. Nature Nanotechnology, 2021. **16**(7): p. 748-759.
17. Garcia-Martin, R., et al., *Tissue differences in the exosomal/small extracellular vesicle proteome and their potential as indicators of altered tissue metabolism*. Cell Reports, 2022. **38**(3): p. 110277.
18. Maia, J., et al., *Exosome-Based Cell-Cell Communication in the Tumor*

- 
- Microenvironment*. *Frontiers in Cell and Developmental Biology*, 2018. **6**.
19. Rodrigues-Junior, D.M., et al., *Extracellular Vesicles and Transforming Growth Factor β Signaling in Cancer*. *Frontiers in Cell and Developmental Biology*, 2022. **10**.
 20. Zhao, H., et al., *Tumor microenvironment derived exosomes pleiotropically modulate cancer cell metabolism*. *eLife*, 2016. **5**: p. e10250.
 21. Yu, D., et al., *Exosomes as a new frontier of cancer liquid biopsy*. *Molecular Cancer*, 2022. **21**(1).
 22. Mukerjee, N., et al., *Exosomes in liquid biopsy and oncology: Nanotechnological interplay and the quest to overcome cancer drug resistance*. *The Journal of Liquid Biopsy*, 2024. **3**: p. 100134.
 23. Lee, B.S., et al., *Crosstalk between head and neck cancer cells and lymphatic endothelial cells promotes tumor metastasis via CXCL5-CXCR2 signaling*. *The FASEB Journal*, 2021. **35**(1).
 24. Committee, C.C.S.A. *Survival statistics for oral cancer*. 2021; Available from: <https://cancer.ca/en/cancer-information/cancer-types/oral/prognosis-and-survival/survival-statistics>.
 25. Paget, S., *THE DISTRIBUTION OF SECONDARY GROWTHS IN CANCER OF THE BREAST*. *The Lancet*, 1889. **133**(3421): p. 571-573.
 26. Ribatti, D., G. Mangialardi, and A. Vacca, *Stephen Paget and the 'seed and soil' theory of metastatic dissemination*. *Clinical and Experimental Medicine*, 2006. **6**(4): p. 145-149.
 27. Hoshino, A., et al., *Tumour exosome integrins determine organotropic metastasis*. *Nature*, 2015. **527**(7578): p. 329-335.
 28. Wang, S.H., et al., *Laminin γ 2-enriched extracellular vesicles of oral squamous cell carcinoma cells enhance *in vitro* lymphangiogenesis via integrin α 3-dependent uptake by lymphatic endothelial cells*. *International Journal of Cancer*, 2019. **144**(11): p. 2795-2810.
 29. Norden, P.R. and T. Kume, *Molecular Mechanisms Controlling Lymphatic Endothelial Junction Integrity*. *Frontiers in Cell and Developmental Biology*, 2021. **8**.
 30. Zhang, F., et al., *Lymphatic Endothelial Cell Junctions: Molecular Regulation in Physiology and Diseases*. *Frontiers in Physiology*, 2020. **11**.
 31. Hasegawa, T., et al., *Cystine reduces tight junction permeability and intestinal inflammation induced by oxidative stress in Caco-2 cells*. *Amino Acids*, 2021. **53**(7): p. 1021-1032.
 32. Scalavino, V., et al., *The Increase of miR-195-5p Reduces Intestinal Permeability in Ulcerative Colitis, Modulating Tight Junctions' Expression*. *International Journal of Molecular Sciences*, 2022. **23**(10): p. 5840.
 33. Tomita, T., M. Kato, and S. Hiratsuka, *Regulation of vascular permeability in cancer metastasis*. *Cancer Science*, 2021. **112**(8): p. 2966-2974.
 34. Dejana, E., *Endothelial cell-cell junctions: happy together*. *Nature Reviews Molecular Cell Biology*, 2004. **5**(4): p. 261-270.
 35. Dun Niu, T.L., Hanbin Wang, Yiniu Xia, Zhizhong Xie, *Lactic acid in tumor invasion*. *Clinica Chimica Acta*, 2021. **522**: p. 61-69.
 36. Kujawa, M., et al., *MicroRNA-466 and microRNA-200 increase endothelial permeability in hyperglycemia by targeting Claudin-5*. *Molecular Therapy - Nucleic Acids*, 2022. **29**: p. 259-271.
 37. Liu, Y., et al., *Integrated bioinformatic analysis of dysregulated microRNA-mRNA*

- co-expression network in ovarian endometriosis. Acta Obstetrica et Gynecologica Scandinavica*, 2022. **101**(10): p. 1074-1084.
38. Sanchez, T., et al., *Induction of Vascular Permeability by the Sphingosine-1-Phosphate Receptor-2 (S1P2R) and its Downstream Effectors ROCK and PTEN. Arteriosclerosis, Thrombosis, and Vascular Biology*, 2007. **27**(6): p. 1312-1318.
39. Li, N., et al., *MiR-106b and miR-93 regulate cell progression by suppression of PTEN via PI3K/Akt pathway in breast cancer. Cell Death & Disease*, 2017. **8**(5): p. e2796-e2796.
40. Bian, L., et al., *MiR-29c-3p and MiR-223-3p regulate the proliferation and drug resistance of oral squamous cell carcinoma by targeting ANGPTL4. Frontiers of Oral and Maxillofacial Medicine*, 2022. **4**.
41. Fan, H., et al., *CircPTK2 Inhibits the Tumorigenesis and Metastasis of Gastric Cancer by Sponging miR-134-5p and Activating CELF2/PTEN Signaling. 2021, Research Square Platform LLC.*
42. Zhang, L., et al., *miR-134-5p Promotes Stage I Lung Adenocarcinoma Metastasis and Chemoresistance by Targeting DAB2. Molecular Therapy - Nucleic Acids*, 2019. **18**: p. 627-637.
43. Zhao, L., et al., *miR-34c Regulates the Permeability of Blood-Tumor Barrier via MAZ-Mediated Expression Changes of ZO-1, Occludin, and Claudin-5. Journal of Cellular Physiology*, 2015. **230**(3): p. 716-731.
44. Minemura, C., et al. *Identification of Antitumor miR-30e-5p Controlled Genes; Diagnostic and Prognostic Biomarkers for Head and Neck Squamous Cell Carcinoma. Genes*, 2022. **13**, DOI: 10.3390/genes13071225.
45. Zongdan, J., et al., *The mechanism of miR-363-3p/DUSP10 signaling pathway involved in the gastric mucosal injury induced by clopidogrel. Toxicology Mechanisms and Methods*, 2021. **31**(2): p. 150-158.
46. Gao, M., et al., *Sepsis plasma-derived exosomal miR-1-3p induces endothelial cell dysfunction by targeting SERP1. Clinical Science*, 2021. **135**(2): p. 347-365.

(A)



(B)

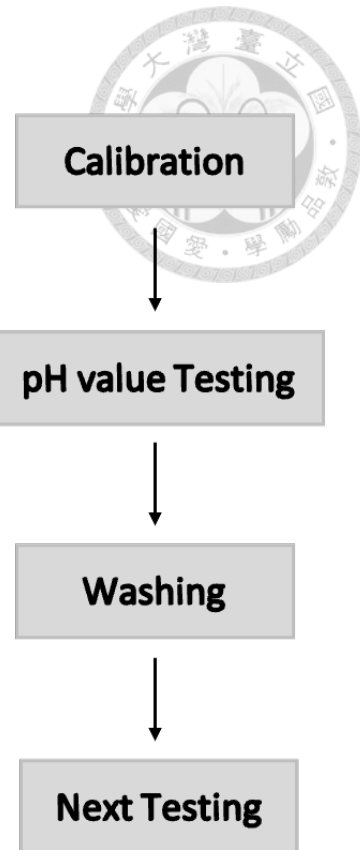
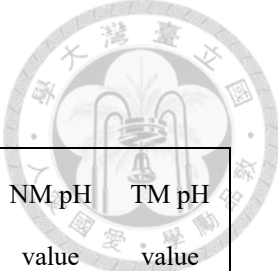


Figure 1. Working setting for pH measurement of clinical oral cancer specimens

(A) HORIBA pocket pH meter appearance and cross-sectional view. Working area setting

for pH measurement. (B) pH measurement workflow.

Table 1. Subject basic information



	Age	Sex	Smoke/ Betel Nut	TNM	N. side pH value	T. side pH value	NM pH value	TM pH value
1	64	F	N/N	pT4aN0M0	7.74	8.1	7.73	7.95
2	59	M	Y/Y	pT2N0M0	7.33	6.84	7.35	7.35
3	63	M	Y/Y	pT4aN0M0	8.2	6.7	6.63	6.33
4	63	M	Y/N	pT1N0M0	6.94	6.68	7.28	6.49
5	37	M	Y/Y	ypT2N0M0	7.88	7.28	7.75	6.06
6	51	M	Y/Y	pT2N0M0	4.89	7.43	3.7	7.65
7	58	M	Y/Y	pT1N0M0	4.37	7.43	4.86	7.4
8	56	M	Y/Y	pT1N0M0	11.29	7.48	9.57	7.45
9	68	F	N/N	pT1N0M0	9.32	7.21	7.47	7.9
10	68	M	N/N	ypT2N3bM0	7.27	6.61	9.32	6.37
11	25	F	Y/N	pT2N1M0	7.17	7.33	7.33	7.18
12	46	M	Y/Y	pT2N0M0	6.39	12.69	10.98	10.6
13	68	F	N/N	pT1N0M0	12.89	8.25	13.81	8.74
14	69	M	Y/Y	ypT1N0M0	9.3	8.7	7.67	5.21
15	64	F	N/N	pT4aN0M0	4.99	10.99	5.03	10.62
16	65	M	Y/Y	ypT4bN0M0	7.29	6.29	7.29	4.98
17	56	M	Y/Y	pT1N0M0	12.63	7.51	12.11	7.16
18	69	M	Y/Y	ypT1N0M0	7.5	6.65	7.46	6.96
19	54	F	N/N	pT2N0M0	7.37	7.24	7.48	7.26
20	54	M	Y/Y	pT2N3bM0	6.31	7.41	6.86	7.3
21	27	F	Y/N	ypT4aN1M0	3.55	9.26	9.49	8.97
22	49	M	Y/Y	ypT2N3bM0	7.03	7.15	7.38	7.13
23	54	M	Y/Y	pT4aN2bM0	6.26	2.68	6.68	2.68
24	69	M	Y/Y	ypT4aN3b	7.18	7.45	5.29	2.85

Note: N. side=Normal Side, T. side=Tumor Side, NM=Normal Mucosa, TM=Tumor Mucosa.

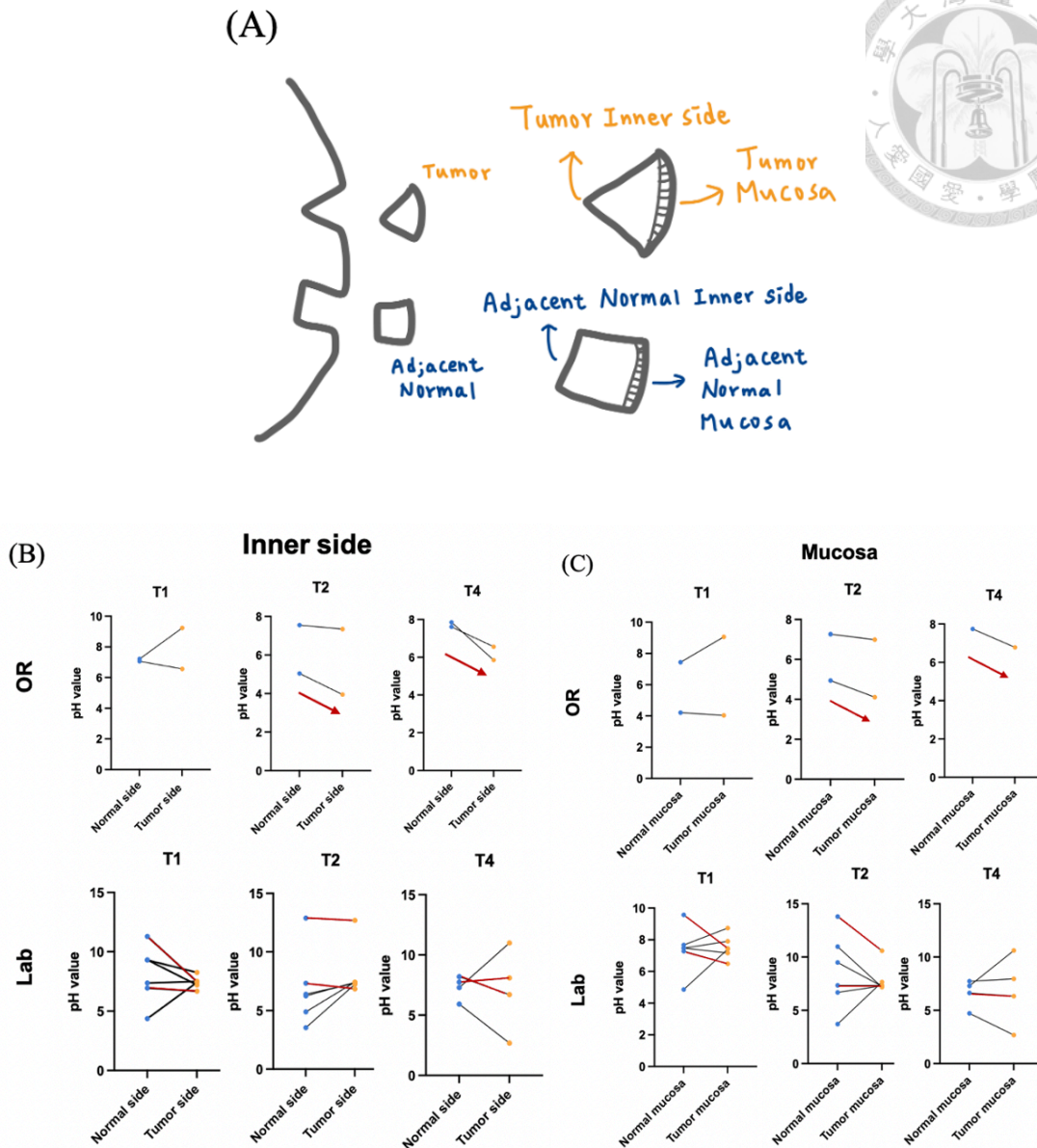


Figure 2. Clinical specimens show decreased pH value in the late stage of cancer

(A) Schematic diagram of collecting the specimen, which is divided into the tumor site and the adjacent normal side. The inner side is the Tumor side/Adjacent Normal side, and the outer side is the mucosa. (B) Group the subjects according to tumor size (T), remove the data of subjects who have been treated (y), then distinguish the values measured in the operating room and laboratory, and compare the pH values of tumor tissue and normal tissue respectively.

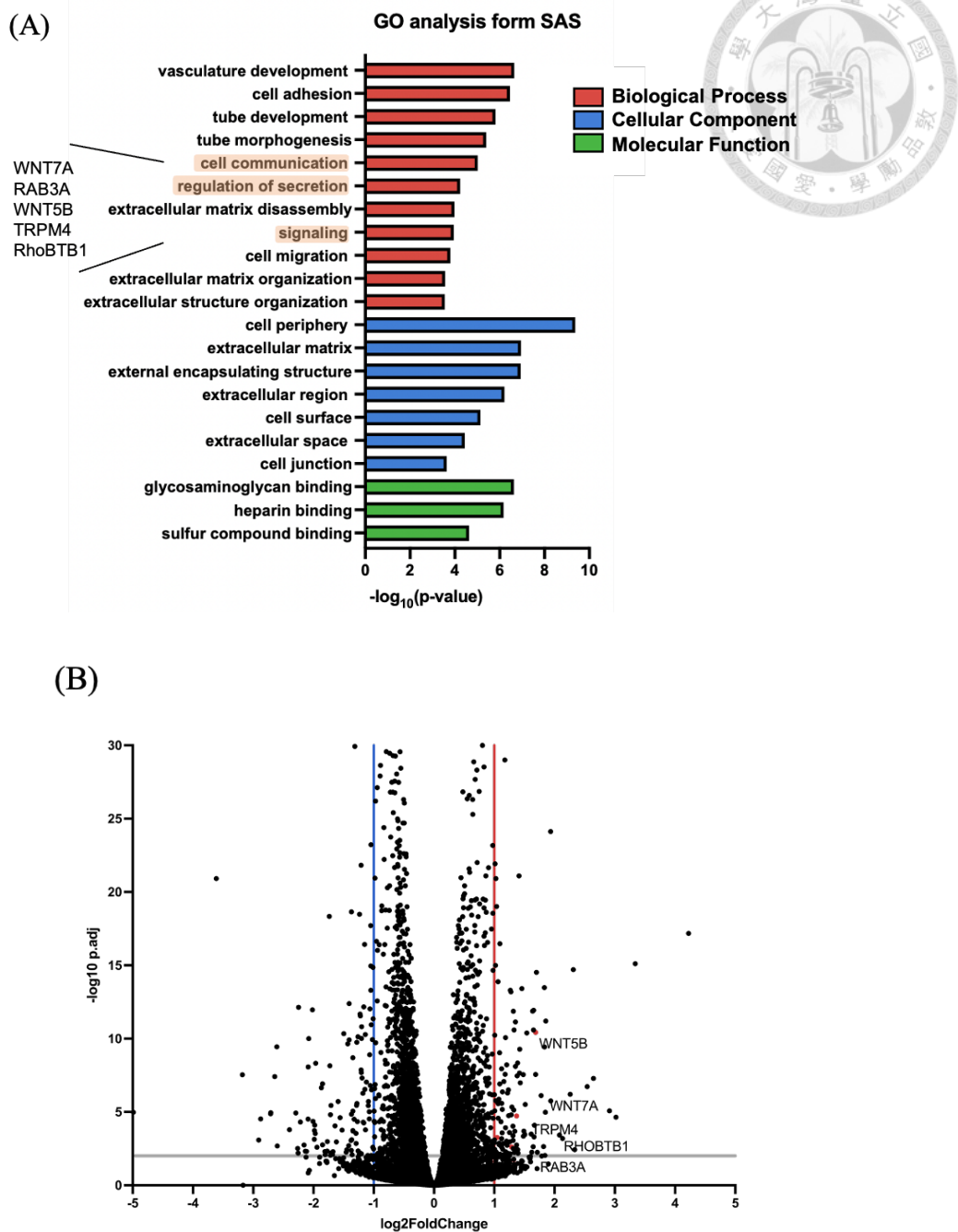


Figure 3. Extracellular vesicle biogenesis-related genes appeared in SAS cell transcriptome

(A) 360 significantly different DEGs from transcriptome revealed that molecular functions related to extracellular matrix interaction, signaling, and secretion abundant in SAS cells. (B) Genes related to extracellular biogenesis function are all up-regulated genes that are located on the right side of the volcano plot.

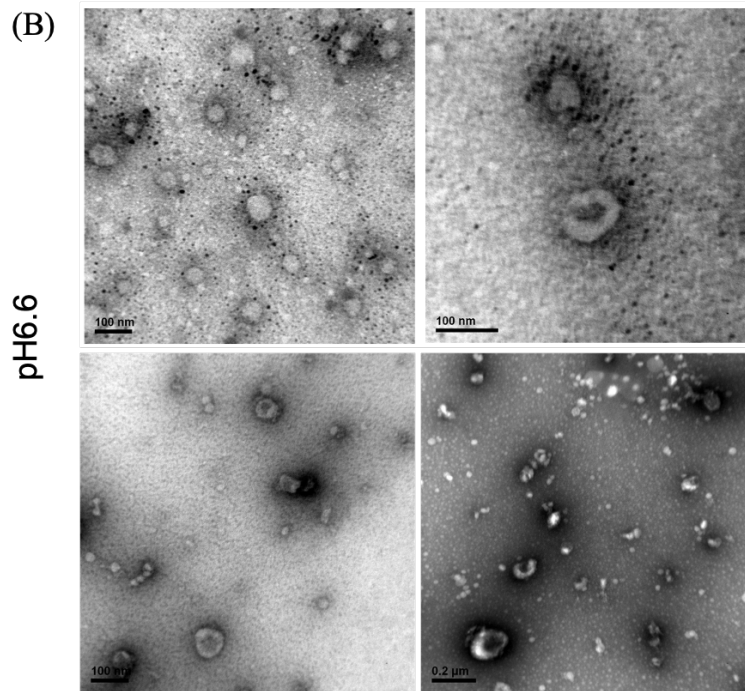
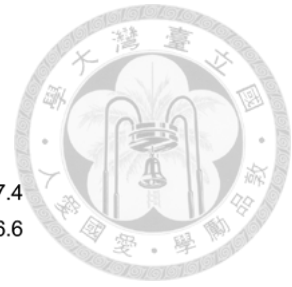
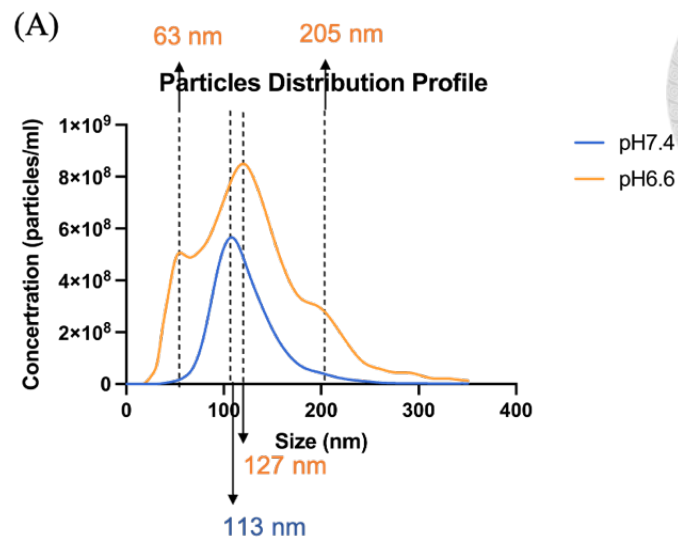


Figure 4. Different characteristics of SAS-derived extracellular vesicles under different pH values.

(A) Extracellular vesicles distribution of size and concentration under pH 7.4 and pH 6.6.

(B) pH 6.6 EV morphology under the transmission electron microscope, classic round, and cup-shaped structure, with a size of approximately around 100 nm.

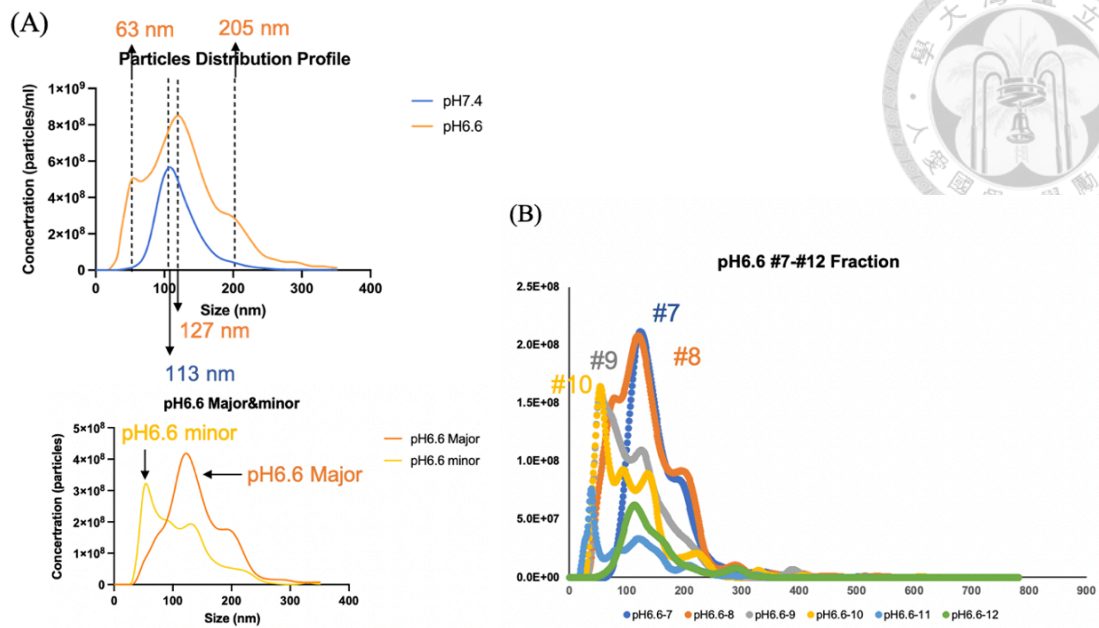


Figure 5. The main population and minor population of pH6.6 EVs can be distinguished from nanoparticle tracking analysis.

(A) The EV population after acidification was different from the pH7.4 group, and different subgroups appeared. (B) The size exclusion NTA results of fractions 7 to 12 could distinguish the major and minor groups by pooling some fractions together.

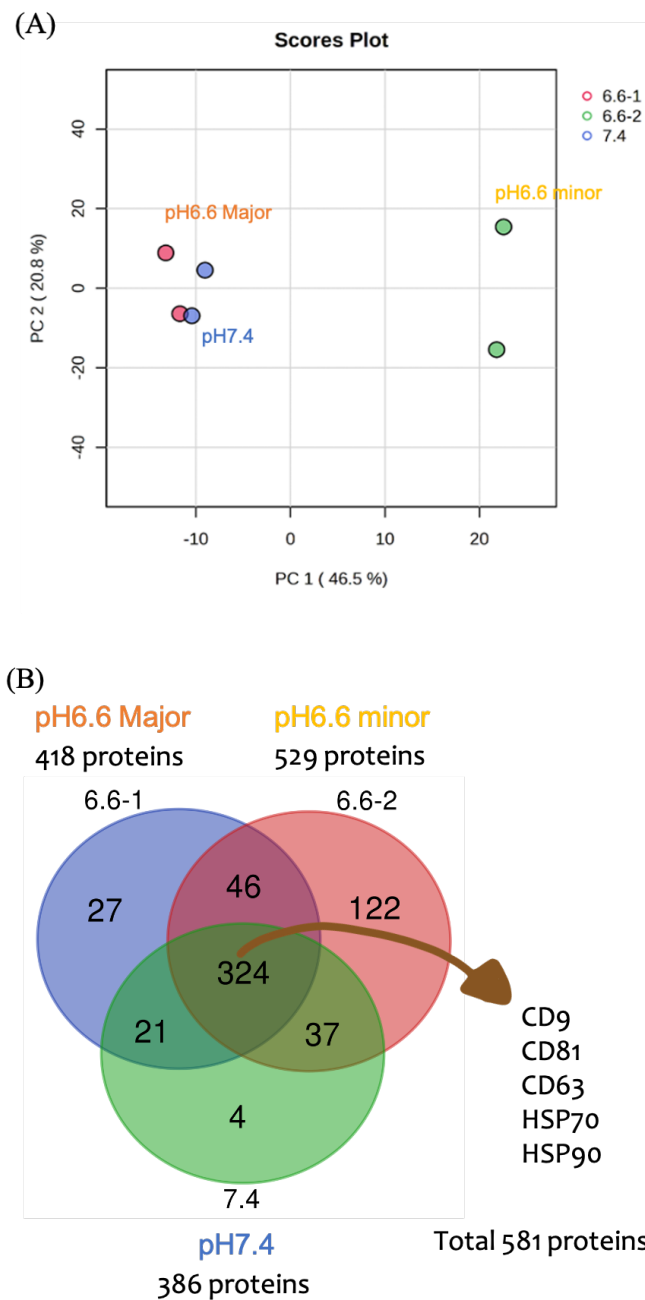


Figure 6. Acidification induces SAS to release the extracellular vesicles with different protein compositions.

(A) Principal Component Analysis (PCA) further indicated a high level of similarity among vesicle populations with comparable sizes. (B) The Venn diagram highlighted substantial protein differences in SAS-released EVs, and the classic protein showed in the overlaps within three groups.

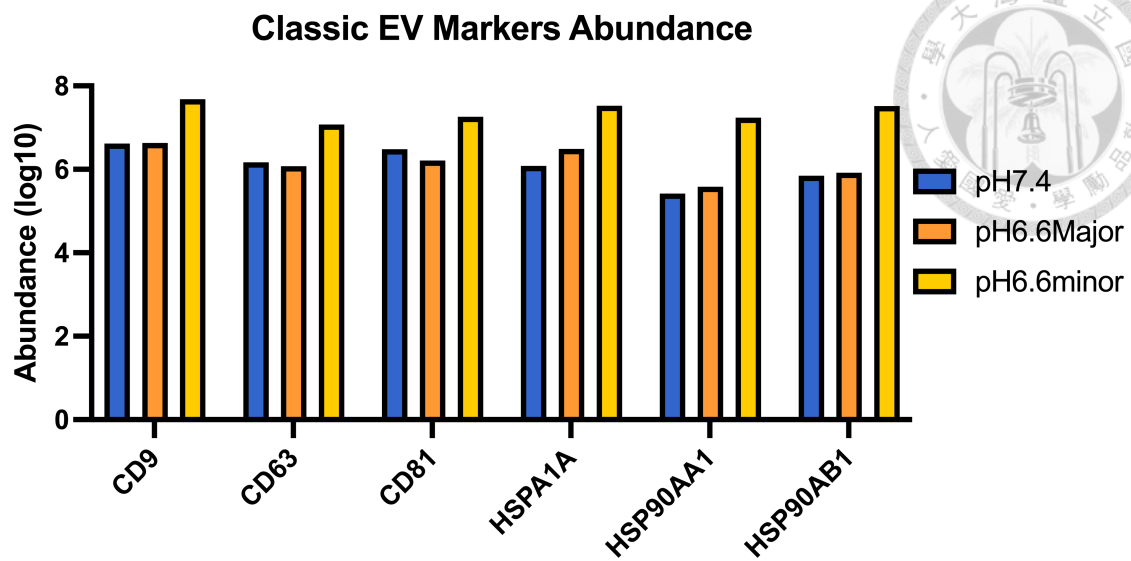
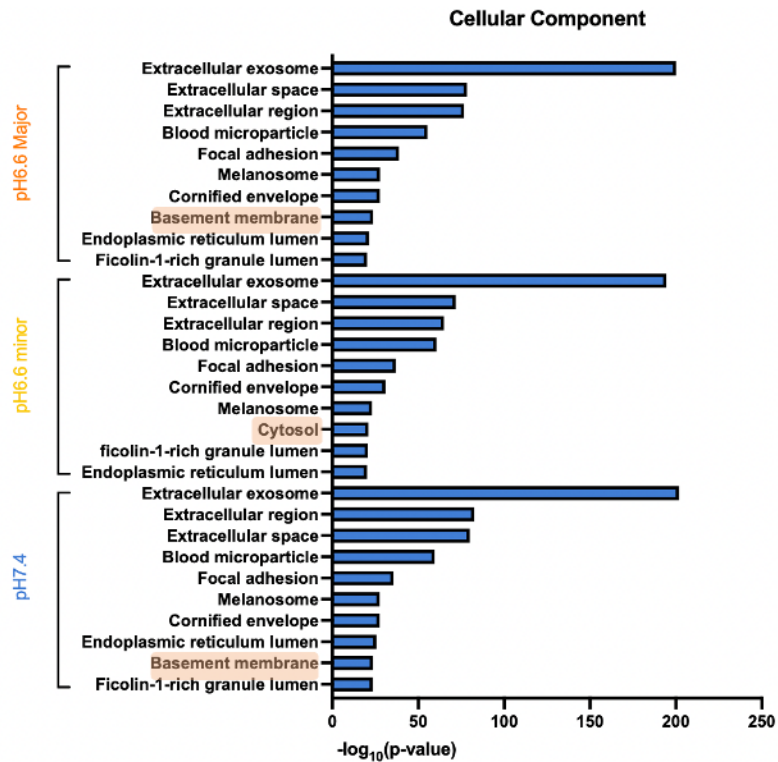
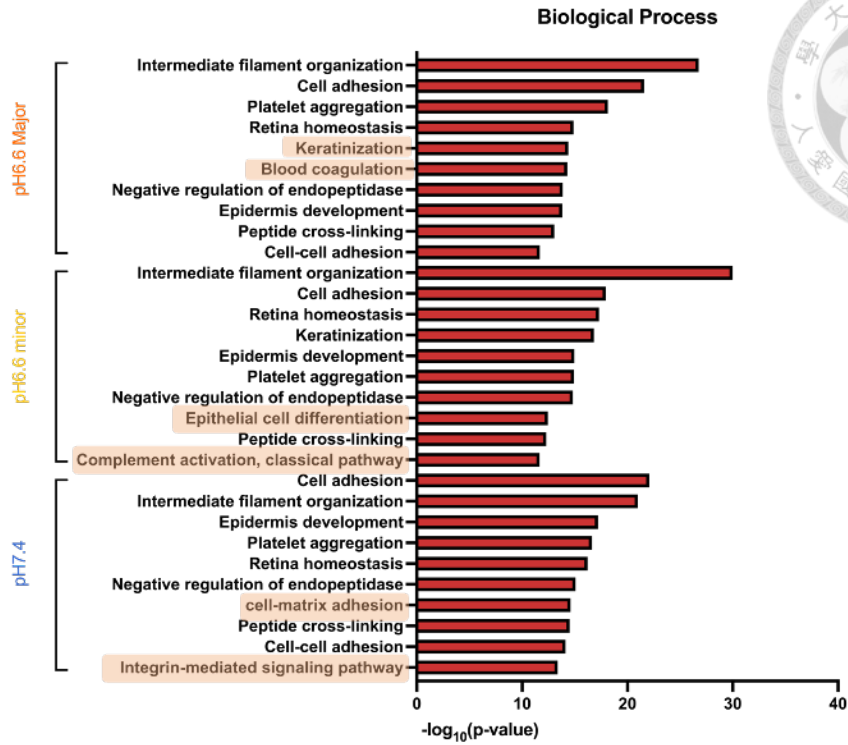


Figure 7. Extracellular vesicles secreted by SAS cells contain typical protein markers. In addition to the transmembrane proteins CD9, CD63, and CD81, the typical extracellular protein HSP70 (HSPA1A) and two variants of HSP90 (HSP90AA1, HSP90AB1) are included. Among them, the content of CD9 is the highest among the three groups, and the content of each typical marker protein is the most abundant in the pH 6.6 Minor group.



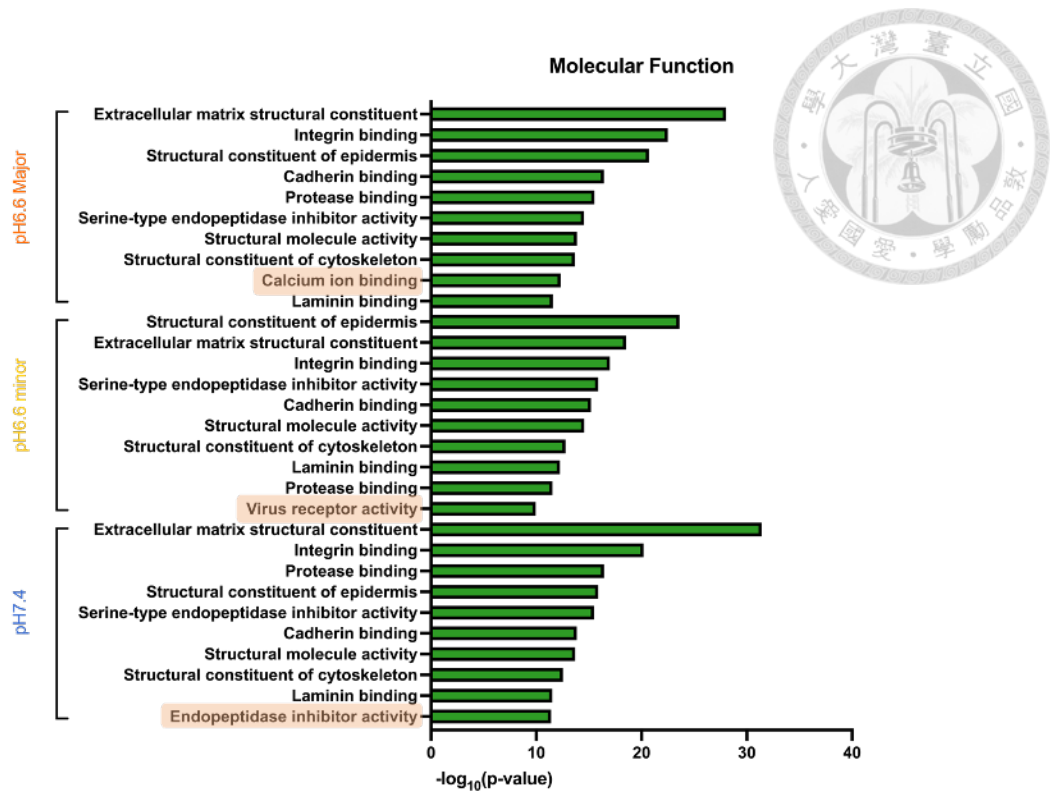


Figure 8. Top 10 enriched GO terms covering biological process, cellular component, and molecule function in SAS extracellular vesicles under different pH conditions.

"Cell adhesion" and "Intermediate Filament organization" are the most significantly different processes in BP. "Extracellular exosome" was observed in CC as the most significant component of the three groups. In addition, there are many components related to extracellular matrix interaction and adhesion functions. In MF, the structure-related functions "Extracellular structural constituent" and "Integrin binding" are the most significant functions.

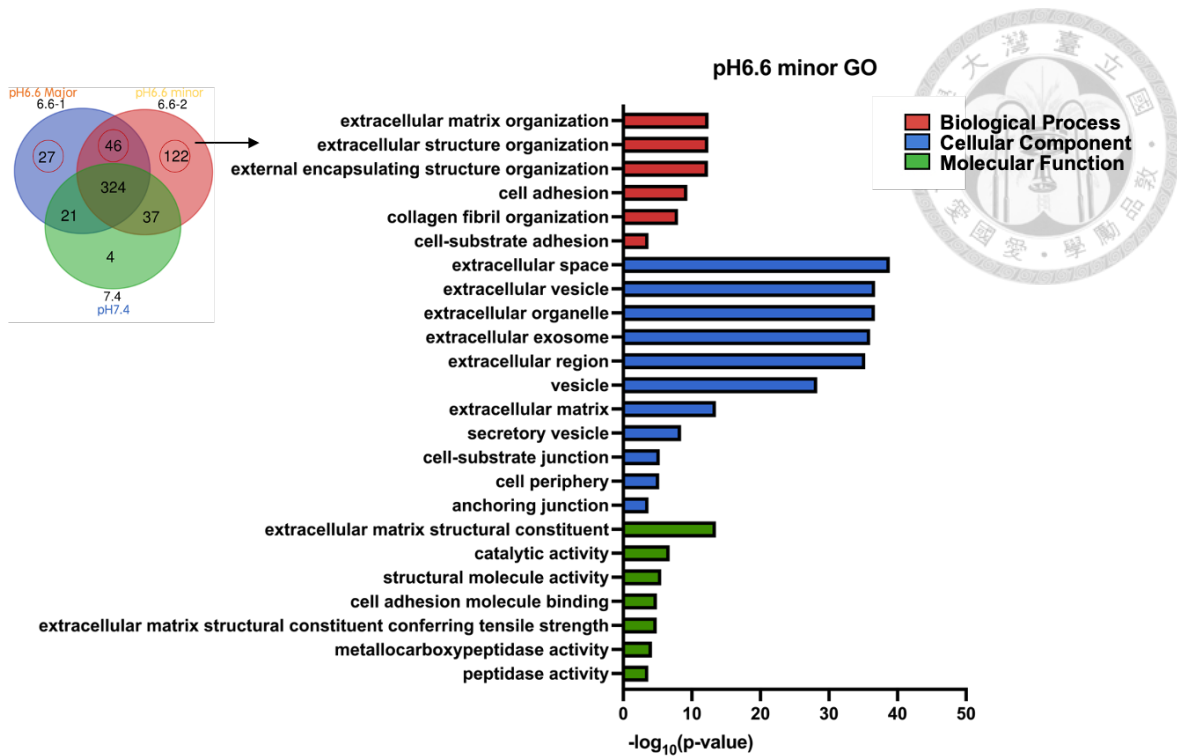


Figure 9. Gene Ontology analyzes the protein function of pH 6.6 Minor.

The protein functions of the pH 6.6 minor group may affect the interaction with the extracellular matrix through the catalytic enzymes and may also regulate adhesion-related functions so that substances outside the cells can easily make contact with cells to achieve physical changes in cell structure.

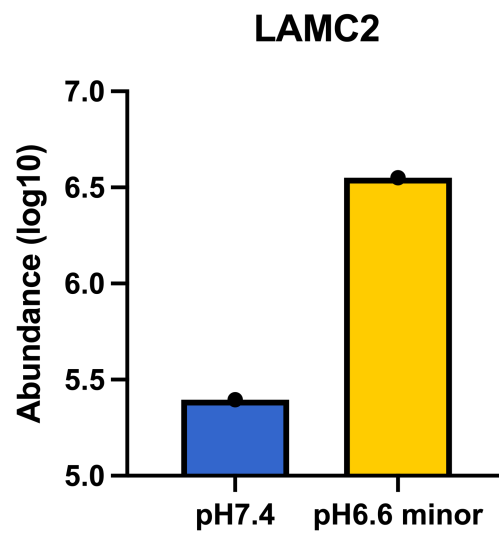


Figure 10. Proteins that can promote EV internalization appeared in the pH6.6 minor group.

Compared with the pH7.4 group, abundant Laminin r3 signals were found on extracellular vesicles in the pH6.6 minor group.

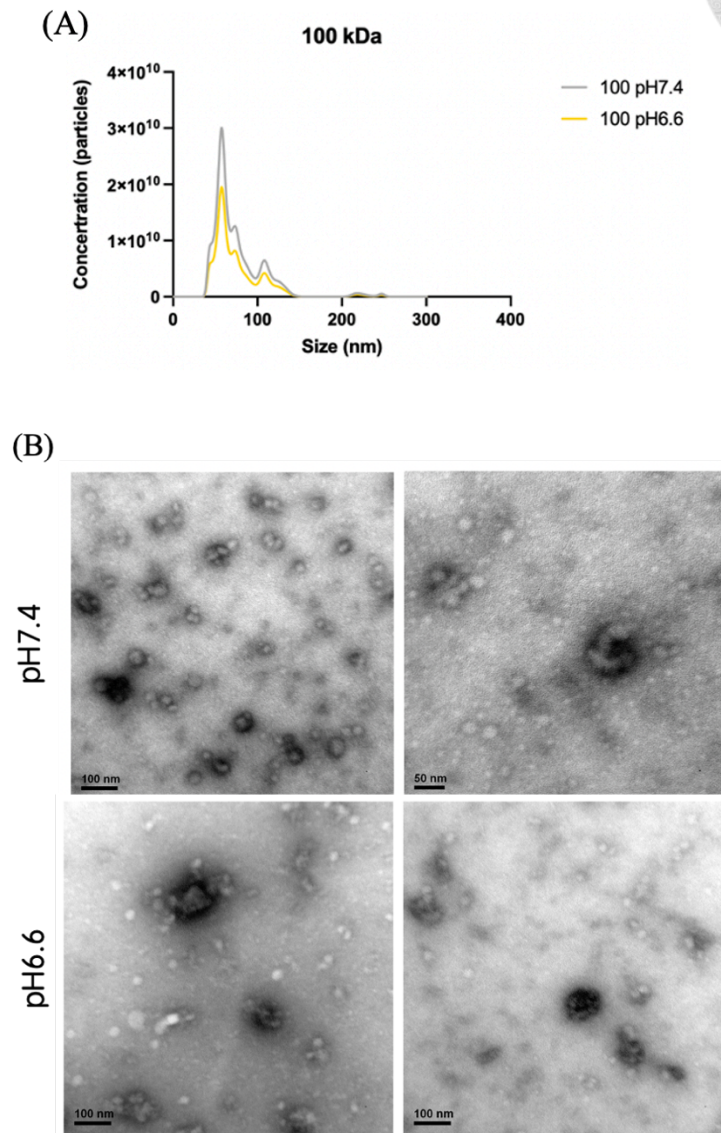


Figure 11. Characteristics of extracellular vesicle isolated by Tangential Flow Filtration

(A) The size and concentration distribution of extracellular vesicles isolated using 100 kDa. (B) TEM observation of extracellular vesicles isolated from TFF 100kDa. Vesicle sizes less than 100 nm can be observed, with round and cup-shaped appearances.

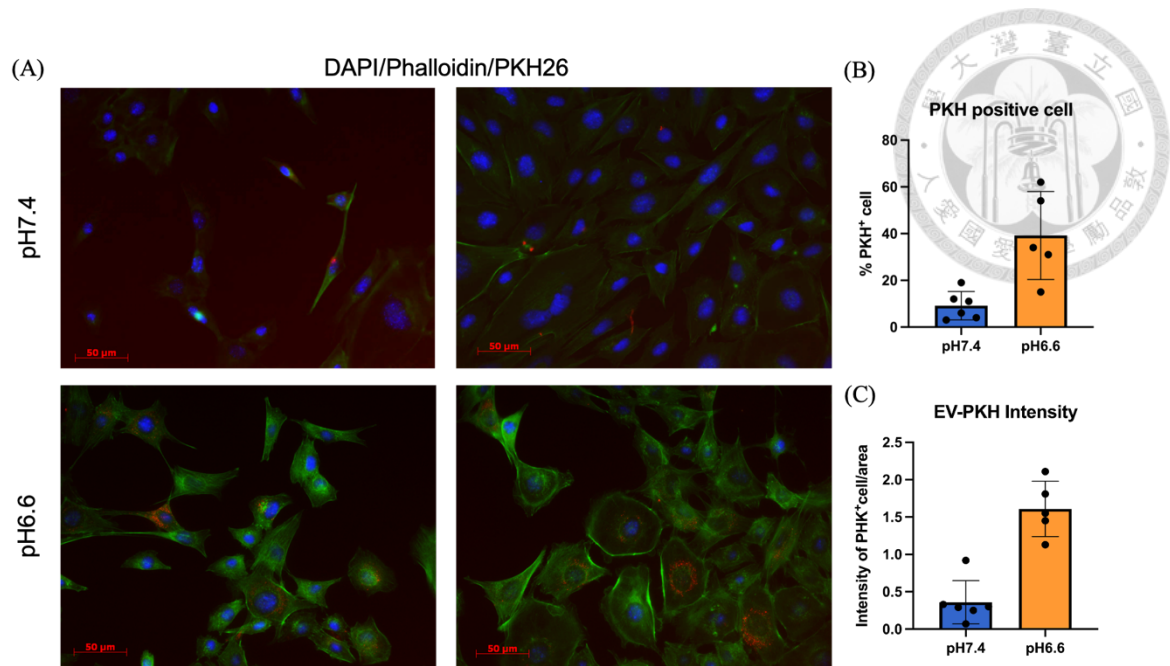


Figure 12. PKH Labeling shows Extracellular Vesicles Retention in Endothelial Cells Under Different pH Values.

(A) Lymphatic endothelial cells tend to retain EVs in the cell after internalization of pH 6.6 EVs, but this phenomenon was not observed when cells internalized pH 7.4 EVs. (B) PKH⁺ cell percentage and (C) PKH⁺ intensity showed the same trend of pH6.6 EV have the retention potential

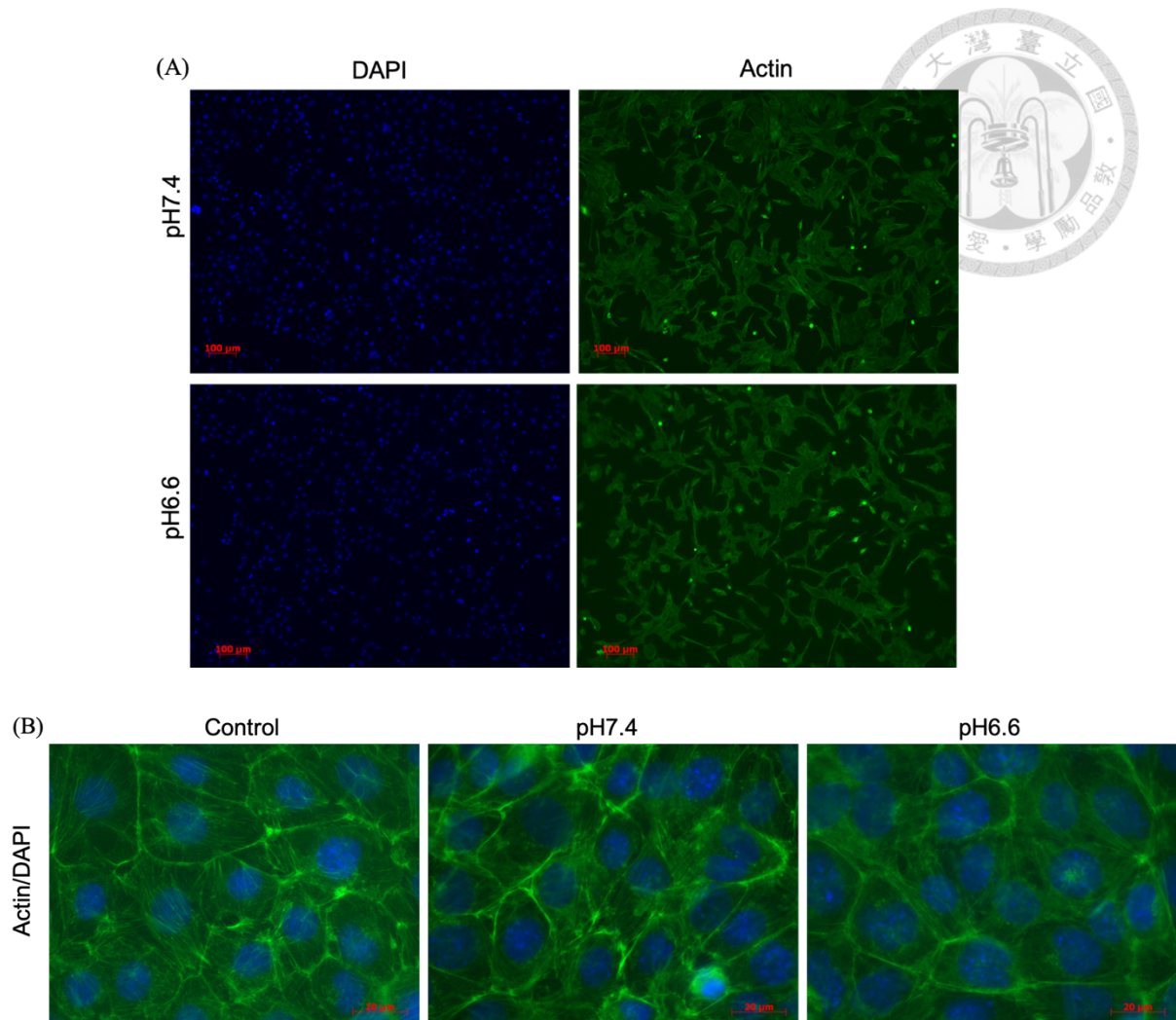


Figure 13. Endothelial cells under EV treatment show no growth difference but different cytoskeleton organization.

(A) Endothelial cells treated with different pH value EVs under low power of view, showed elongated, shrunk cellular structure in pH 6.6. (B) The control group had clear cell boundaries and skeleton signals, but the signals at the cell boundaries in the EV-treated group were somewhat blurry.

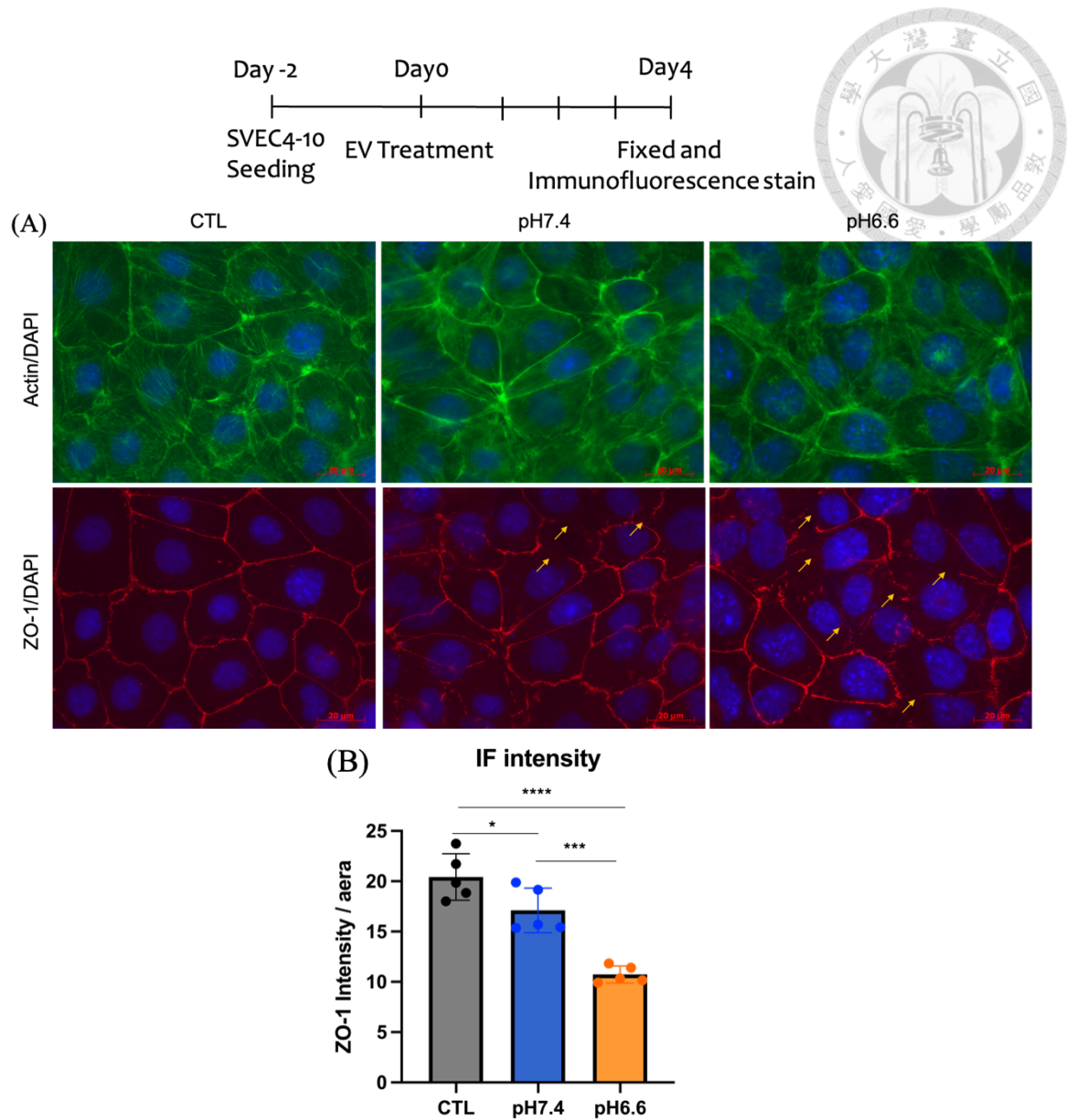


Figure 14. Immunofluorescence staining revealed a disruption in tight junction ZO-1 expression in the extracellular vesicles-treated group.

(A) Under the immunofluorescence, fragmented ZO-1 signals were evident in both the pH7.4 and pH6.6 groups, compared to the control group. Among that, the pH6.6 group exhibited more significant fragmentation. (B) Fluorescence quantification was utilized to verify the fluorescence signal intensity, and the fluorescence intensity was calculated from five different fields.

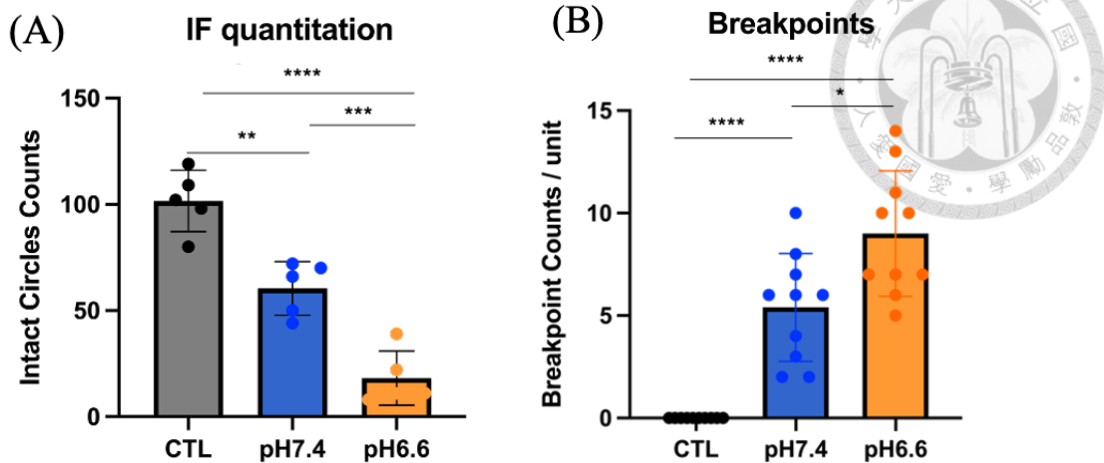


Figure 15. Using Different Quantitation Methods of Lymphatic Endothelial Cell ZO-1 signals under Different pH values show the same trend.

(A) The number of complete circles formed by ZO-1 was counted. (B) The count of breakpoints at a fixed length (26 μm). Among the three groups, pH 6.6 demonstrated the highest counts of incomplete cell boundaries. (*= $p < 0.05$, **= $p > 0.001$, ***= $p < 0.0005$, ****= $p < 0.0001$)

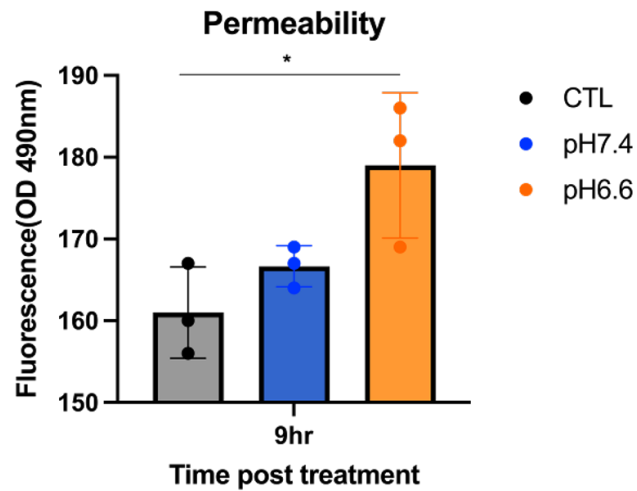
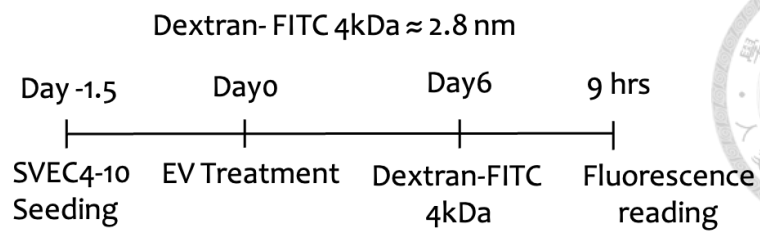


Figure 16. Evaluating the permeability of the lymphatic endothelial cell barrier through tracking FITC-dextran across the membrane.

The fluorescence intensity of FITC in the basolateral (BL) of Dextran-FITC 4kDa was measured, revealing that the group subjected to pH 6.6 treatment exhibited the highest permeability.

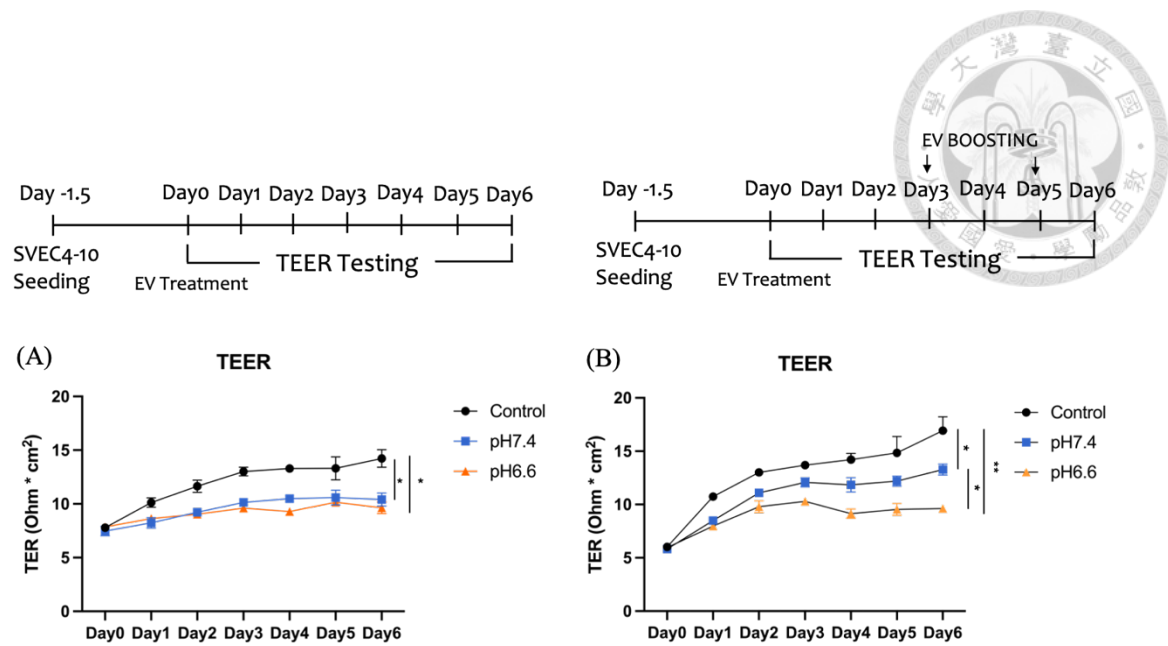


Figure 17. Trans Endothelial Electric Resistance (TEER) detects the resistance of the endothelial barrier.

(A) Endothelial cell barrier integrity changes after different pH values in extracellular vesicle treatment which resulted in a lower resistance than the control group. (B) EV doses boosting to simulate physiological scenarios.

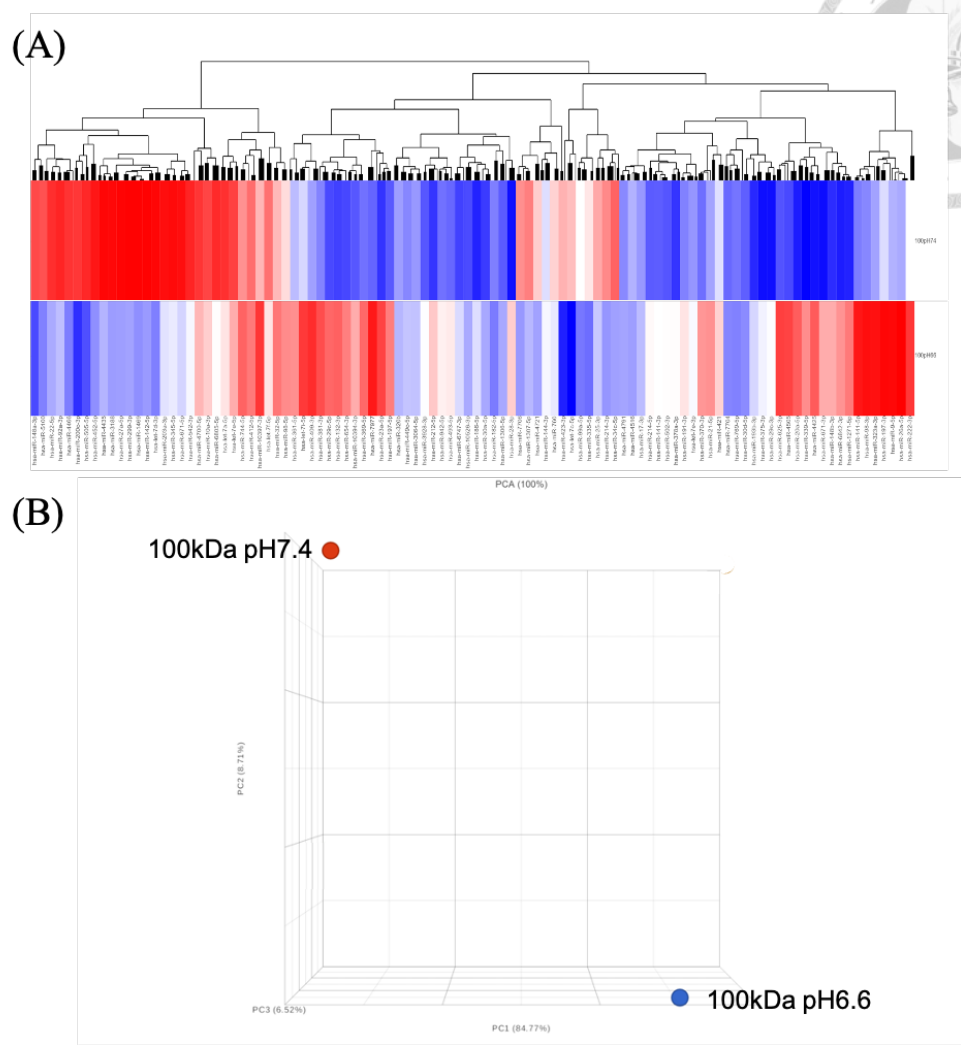
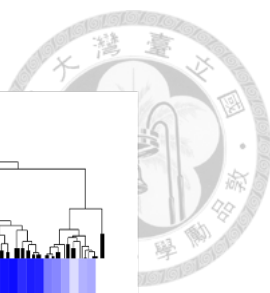


Figure 18. Differences in the composition of miRNA between 100kDa pH 7.4 and pH 6.6. (A) Analysis of the extracellular miRNA composition of the two groups at different pH values reveals distinctions. Similar results are also evident in (B) PCA analysis.

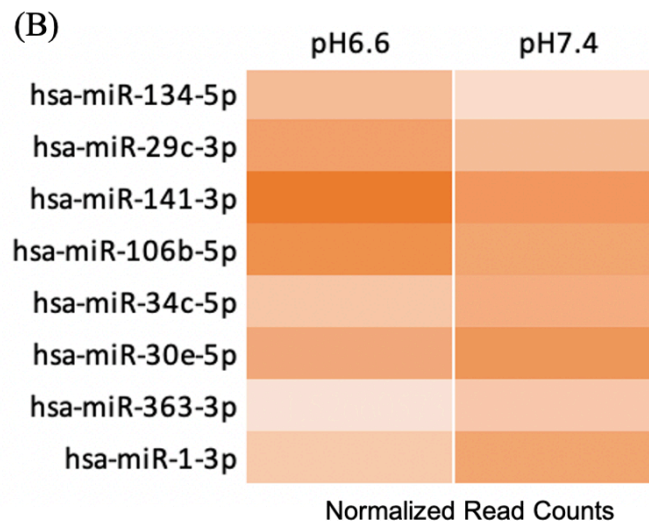
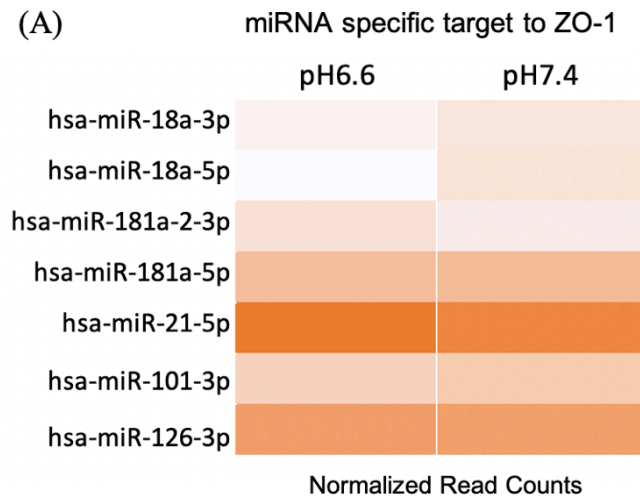


Figure 19. miRNAs specific target to ZO-1 appear in extracellular vesicles at both pH values

(A) We identified the miRNAs specific target to ZO-1 protein. Identify seven miRNAs that have been reported in the past and they appear in both pH values and reflect the cell barrier experiments that both cause ZO-1 damage. (B) miRNAs of cytoskeleton regulation and junction breaking are also found in oral cancer extracellular vesicles.